Pulling a polymer with anisotropic stiffness near a sticky wall

2012 J. Phys. A: Math. Theor. 45 435002

(http://iopscience.iop.org/1751-8121/45/43/435002)

IOP Publishing Journal of Physics A: Mathematical and Theoretical

J. Phys. A: Math. Theor. **45** (2012) 435002 (40pp) doi:10.1088/1751-8113/45/43/435002

Pulling a polymer with anisotropic stiffness near a sticky wall

R Tabbara and A L Owczarek

Department of Mathematics and Statistics, The University of Melbourne, Victoria 3010, Australia

E-mail: tabbarar@ms.unimelb.edu.au and a.owczarek@ms.unimelb.edu.au

Received 24 July 2012, in final form 17 September 2012
Published 10 October 2012
Online at stacks.iop.org/JPhysA/45/435002

Abstract

We solve exactly a two-dimensional partially directed walk model of a semi-flexible polymer that has one end tethered to a sticky wall, while a pulling force away from the adsorbing surface acts on the free end of the walk. This model generalizes a number of previously considered adsorption models by incorporating individual horizontal and vertical stiffness effects, in competition with a variable pulling angle. A solution to the corresponding generating function is found by means of the kernel method. While the phases and related phase transitions are similar in nature to those found previously the analysis of the model in terms of its physical variables highlights various novel structures in the shapes of the phase diagrams and related behaviour of the polymer. We review the results of previously considered sub-cases, augmenting these findings to include analysis with respect to the model's physical variables—namely, temperature, pulling force, pulling angle away from the surface, stiffness strength and the ratio of vertical to horizontal stiffness potentials, with our subsequent analysis for the general model focusing on the effect that stiffness has on this pulling angle range. In analysing the model with stiffness we also pay special attention to the case where only vertical stiffness is included. The physical analysis of this case reveals behaviour more closely resembling that of an upward pulling force acting on a polymer than it does of a model where horizontal stiffness acts. The stiffness–temperature phase diagram exhibits re-entrance for low temperatures, previously only seen for three-dimensional or co-polymer models. For the most general model we delineate the shift in the physical behaviour as we change the ratio of vertical to horizontal stiffness between the horizontal-only and the vertical-only stiffness regimes. We find that a number of distinct physical characteristics will only be observed for a model where the vertical stiffness dominates the horizontal stiffness.

PACS numbers: 05.50.+q, 05.70.Fh, 61.41.+e

(Some figures may appear in colour only in the online journal)

1. Introduction

The competition of a pulling force with an adsorbing potential at a wall on the behaviour of single polymers in solution has been the subject of continued recent interest [5, 11, 13, 19, 21, 24, 32]. This has been in part due to the advent of experimental techniques able to micro-manipulate single polymers [1, 33, 34] and the connection to modelling DNA denaturation [7, 14–18, 22]. The addition of stiffness to a model of polymers in solution (semi-flexible polymers), which adds an important ingredient to such modelling, has demonstrated non-trivial and interesting results [8, 9, 12, 20, 27, 30] in a variety of contexts.

Over the past few years exactly solvable models of polymers attached to a wall in two and three dimensions incorporating various aspects of adsorption, forces along (horizontal) and away (vertical) from the wall and stiffness have been analysed [10, 23–26, 28].

In this paper, we model the stretching of a polymer in a dilute solution near an attractive surface as a partially directed walk (PDW) in two dimensions, incorporating the individual effects of both horizontal and vertical stiffness. While the inclusion of distinct horizontal and vertical stiffness parameters is not motivated by previous experimental findings, such a model generalizes a host of previously studied and unconsidered stiffness adsorption models, providing the opportunity to understand the overarching effects of stiffness to polymer adsorption.

We begin in section 2 by formally defining our model, building it up from the simple adsorption-only case. We review the key findings of previously considered sub-cases of our generalized model, particularly with respect to the model's physical variables: T temperature, F pulling force and θ the pulling angle away from the surface.

In section 3, we establish a bijection between the class of allowed walks of any length ending at a fixed height onto itself. This leads to a functional equation for the model's corresponding generating function, which is subsequently solved by means of the *kernel method* [2, 4].

We then proceed to locate the radius of convergence of the generating function in section 4 as a function of the system parameters. We identify three relevant singularities in the generating function that for different ranges of the system parameters give rise to the radius of convergence and correspond to the adsorbed, desorbed and stretched phases of the system. This allows us in section 5 to introduce and analyse a general stiffness model that incorporates *proportional* horizontal and vertical stiffness. In particular, we specify a parameter r related to the ratio between the potential energy attributed to vertical stiffness to horizontal stiffness ranging from $r = 0$ which corresponds to a horizontal-only stiffness model, through $r = 0.5$ where we have equal horizontal and vertical stiffness; and to $r = 1$ which coincides with a model having only vertical stiffness. In instances where we either exclude or include pulling, we find that for all $0 \leqslant r \leqslant 1$ the general stiffness model exhibits a second or first-order adsorption phase transition respectively, allowing us to conclude that stiffness effects do not alter the order of the phase transition.

The form of the phase boundaries of the general stiffness model is delineated in section 6, by first considering the previously studied equal ($r = 0.5$) and horizontal-only ($r = 0$) stiffness models in sections 6.2 and 6.3 respectively, extending previous findings, by additionally considering the effects of a variable pulling angle on the model's critical behaviour. Specifically, we find in both cases, for large enough stiffness, that an increase in stiffness *increases* the range of pulling angles that can induce both adsorption and desorption given enough pulling force.

In sections 6.4.1 and 6.4.2, we further study the sub-case of *vertical-only* stiffness ($r = 1$) both without and with pulling respectively which has not previously been studied. We find that

the behaviour of the vertical-only stiffness model with respect to its physical variables differs significantly from previously studied stiffness models, with a stiffness–temperature critical curve that exhibits re-entrance at low temperature and a decreasing slope for large enough T. This allows us to find an upper-bound on the potential energy attributed to vertical stiffness beyond which *no* phase transition is observed. Moreover, while the inclusion of pulling shows that an increase in stiffness similarly *increases* the range of pulling angles that can induce both adsorption and desorption, we find differing characteristics compared to both the horizontal-only and equal stiffness models, further highlighting the distinct nature of the vertical-only stiffness sub-case.

Finally, understanding the extreme stiffness ratio sub-cases of the general model, we proceed in section 6.5 to analyse the model for a general ratio $0 \leqslant r \leqslant 1$. Specifically, we find that the physical behaviour of such a model both with and without pulling is well represented by the horizontal-only and equal stiffness cases when there is a greater energy attributed to horizontal relative to vertical stiffness ($0 \leqslant r \leqslant 0.5$). In particular, for $0 \leqslant r \leqslant 0.5$, we again observe that an increase in stiffness, results in an increase in both the zero-force critical temperature as well as the range of pulling angles that can induce both adsorption and desorption given enough pulling force. This might suggest that when vertical stiffness effects dominate ($0.5 < r < 1$), we should alternatively expect the general model to exhibit behaviour that is similar to the vertical-only stiffness ($r = 1$) model. Indeed, we find that when ignoring pulling, such a model exhibits a zero-temperature critical point along with a maximal critical stiffness, agreeing with the vertical-only stiffness case. However, in contrast, the model with pulling for $0.5 < r < 1$ exhibits physical characteristics of *both* the horizontal-only and vertical-only stiffness models for low and high stiffness respectively, with such features attributed to the latter model dominating as $r \to 1$.

2. Review and the model

2.1. Introduction of the physical parameters

Consider a walk along a square integer lattice that is composed of L steps. The walk begins at the origin $(0, 0)$, while a one-dimensional surface at $y = 0$ restricts the walk to lie in the upper half-plane, $\mathbb{Z} \times \mathbb{Z}_{\geqslant 0}$. Moreover, we require that the walk be *partially directed*, which imposes the constraint that steps in the walk can only be in the $(1, 0)$, $(0, 1)$ and $(0, -1)$ directions. While partial-directedness restricts horizontal steps to lie only in the positive direction $(1, 0)$, we additionally require that the walk be *self-avoiding* solely to guarantee that a vertical step up (down) is not immediately followed by a vertical step down (up). Finally, for computational convenience, we require both the starting and ending steps of the walk to be in the positive horizontal direction $(1, 0)$. An example of an allowable walk meeting all our constraints can be seen in figure 1. We will denote the class of such allowable walks of length L as $\mathcal{W}_L$.

Having defined which walks may be observed within our system, we can now define physical variables along with corresponding Boltzmann factors that capture the desired effects of polymer adsorption, stiffness and pulling. For a given walk $w \in \mathcal{W}_L$, we start by defining a *surface visit step* to be a step in w that lies along the surface $y = 0$. We attribute each such step with a potential energy gain of $-J$, and thus if w contains k surface visit steps then the overall energy change due to surface contacts is $-k(w)J$. This introduces a Boltzmann factor

$$\kappa := \mathrm{e}^{J/T}. \tag{1}$$

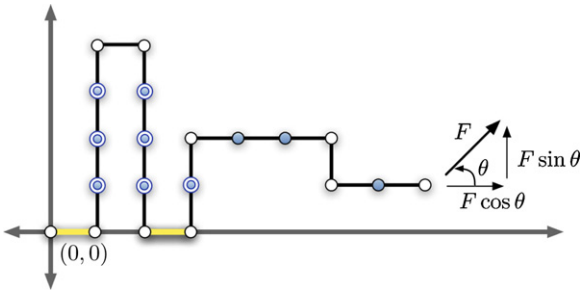

Figure 1. An example of an allowed walk consisting of 8 horizontal and 11 vertical steps (total length $L = 19$), ending at height 1. A force F at an angle θ acts of the end of the polymer as shown. The position of the final site of the walk is at $(h_x, h_y) = (8, 1)$. Note, that both the starting and ending steps must be horizontal. Here, we have $k = 2$ surface visit steps, $\ell_x = 3$ horizontal stiffness sites (filled circles) and $\ell_y = 7$ vertical stiffness sites (circles with filled inner circles). Thus, our overall Boltzmann weight for this configuration in our general model is $\kappa^2\sigma_x{}^3\sigma_y{}^7\mu_x{}^8\mu_y$.

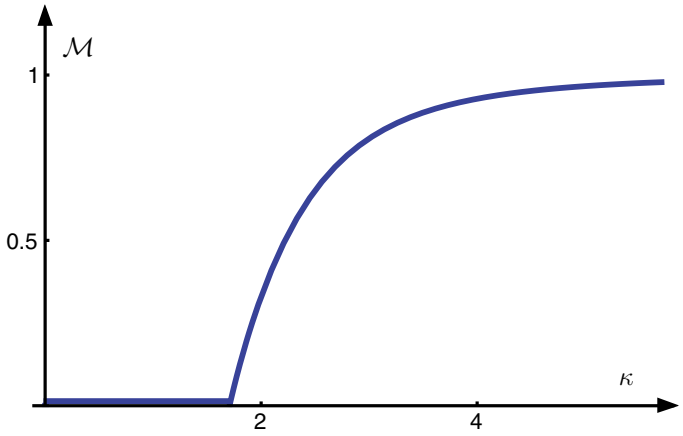

Figure 2. The adsorption only model: a plot of the order parameter $\mathcal{M}$ as function of the surface contact weight κ. The location of the critical point occurs at $\kappa_c = 1 + \frac{1}{\sqrt{2}}$.

For convenience we shall always normalize the Boltzmann constant k_B to 1. The behaviour of a model incorporating this surface contact energy can be described by introducing the *limiting average* fraction of adsorbed surface steps of the polymer $\mathcal{M}$ as

$$\mathcal{M} = \lim_{L\to\infty} \left\langle \frac{k}{L} \right\rangle . \tag{2}$$

As such we can characterize the system as lying in a *desorbed phase* when $\mathcal{M} = 0$, or an *adsorbed phase* when $\mathcal{M} > 0$. Indeed, earlier exact solutions to the adsorption-only model featuring in [3, 6, 31] found that the model exhibits a *second-order adsorption* phase transition, with a finite-jump discontinuity in the second-order derivative of the free energy $(\partial\mathcal{M}/\partial\kappa)$ at the critical point as can be seen in figure 2.

Next, we define F and θ to be the pulling force and angle acting on the free end of the polymer as is seen in figure 1. More precisely, we define $-F$ as the change in elastic energy due to the work performed by stretching the polymer over a unit distance, which we decompose into corresponding horizontal and vertical contributions $-F\sin\theta$ and $-F\cos\theta$, respectively. Thus, if $(h_x, h_y) \in \mathbb{Z} \times \mathbb{Z}_{\geqslant 0}$ are the coordinates of the site in w that is right-most

adjacent to the final step in the walk, then the overall energy change due to vertical pulling is $-h_y(w)F\sin\theta$. Moreover, as our class of walks are partially-directed, w must consist of h_x positive horizontal steps and thus the overall energy change due to horizontal pulling is $-h_x(w)F\cos\theta$. Boltzmann factors

$$\mu_x := \mathrm{e}^{F\cos\theta/T} \tag{3}$$

and

$$\mu_y := \mathrm{e}^{F\sin\theta/T} \tag{4}$$

can then be defined. Such a model, along with variants, have been looked at extensively in both two and three dimensions in [23, 24] and [28], with the latter providing a more in-depth analysis with respect to the exactly solved model's physical variables. It was observed that a shift in the cross-over exponent occurs when a non-zero vertical force ($\mu_y > 1$) is applied to the end of the polymer, indicative of a change in the order of the adsorption transition. Indeed, the transition was found to move from second to first order with the addition of pulling. By introducing a second order parameter $\mathcal{R}$ to be the *limiting average* ratio of final step height to polymer length, that is

$$\mathcal{R} = \lim_{L\to\infty}\left\langle\frac{h_y}{L}\right\rangle, \tag{5}$$

we can catalogue the phases of our system as

- a *desorbed* phase when $\mathcal{M} = \mathcal{R} = 0$,
- a *stretched* phase when $\mathcal{M} = 0$, $\mathcal{R} > 0$,
- while an *adsorbed* phase is observed when $\mathcal{M} > 0$ and $\mathcal{R} = 0$.

The change in the order of the adsorption phase transition with the inclusion of vertical pulling is reflected in the system now shifting from a *stretched* to an adsorbed phase on lowering the temperature, as is seen in figure 3. Therefore, the phase transition from desorbed to adsorbed is second-order, as mentioned above, while the stretched to adsorbed transition is first order: we will find this always holds true in our model.

In both [28] and [29], the inclusion of a variable pulling angle parameter allowed for the possibility of a non-zero pulling force to alternatively induce *adsorption* for pulling angles ranging from 0° to an upper-bound *separating* angle $\theta^s \approx 26.6^\circ$ *for any* non-zero pulling force, as is seen in figure 4. Here, at the separating angle the curve exhibits a purely vertical slope at zero force. Note, that any two critical curves at different pulling angles cannot intersect each other at non-zero force. Thus, any force–temperature critical curve that lies immediately to the right of the separating angle curve must have positive slope at zero-force, and will moreover *always* continue to lie to the right of the separating angle critical curve for any pulling force. Thus, indeed all angles between 0° and θ^s will induce adsorption given enough force. However, contrastingly, pulling a polymer at angles between θ^s and 90° does *not* always induce desorption for all pulling force. Firstly, we note that when $\theta = 45^\circ$, the corresponding force–temperature critical curve exhibits a purely vertical slope as $F \to \infty$. Thus, given this limiting behaviour of the critical curve pulled at 45°, curves that are pulled at angles between the separating angle θ^s and 45° can induce *either* adsorption or desorption depending on the pulling force. A critical curve wedged within this pulling range must have a negative slope at zero-force as it lies to left of the separating angle curve. However, its gradient can not continue to be negative for all F as that would imply it would intersect the critical curve corresponding to a pulling angle of 45°. Additionally, we assert that the slope of critical curves at pulling angles below 45°, including the separating angle curve, must eventually be *positive* for large F. At these angles, pulling a walk places a greater weight on horizontal relative to

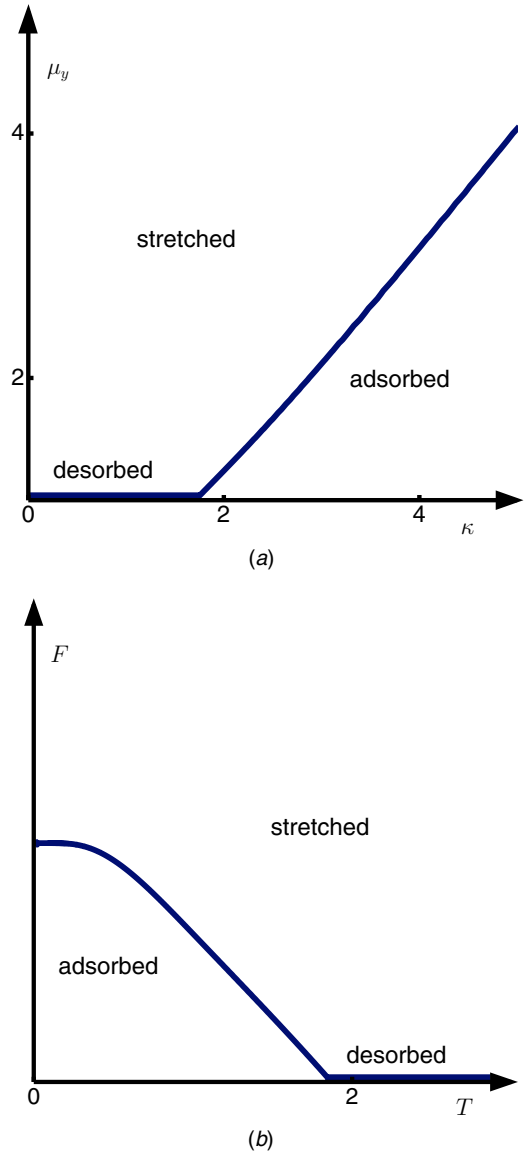

Figure 3. The model with vertical pulling and no stiffness effects: the critical curve for the adsorption phase transition plotted in terms of (*a*) the Boltzmann factors μ_y (vertical pulling weight) against κ (surface attraction weight); and in terms of (*b*) the physical variables F (vertical pulling force) against T (temperature).

vertical steps, favouring adsorption. Therefore, as the pulling force increases, so too must the temperature for the system to remain in a stretched phase. An example of a critical curve that induces both adsorption and desorption can be seen in figure 5 showing the effect of pulling a polymer at 40° which lies between $\theta^s \approx 26.6°$ and 45°. In figure 5(*a*) we expectantly observe that the force–temperature curve lies to the left of the separating angle curve, exhibiting a positive slope for large F. Indeed, such behaviour can be more clearly seen by restricting the temperature domain in figure 5(*b*), where we additionally highlight the separation of the

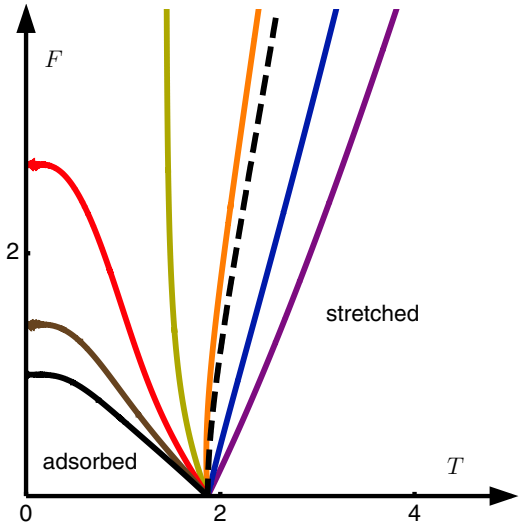

Figure 4. The model with pulling and no stiffness effects: the temperature–force critical curve at different pulling angles. For each plot, starting from the right-most (purple) curve, the individual curves corresponding to an upward pulling angle of 0°, 15°, 30°, 45°, 60°, 75° and 90° away from the surface respectively. Additionally, the dashed curve corresponds to a *separating* pulling angle of $\tan^{-1}(1/2) \approx 26.6°$. Note that the high temperature phase is *desorbed* when $F = 0$ and the transition is second rather than first order.

phases, which is justified by plotting the order parameter $\mathcal{M}$ with respect to the physical variables in figure 5(*c*). Thus, pulling a polymer at an angle between 0° up to $\theta^s \approx 26.6°$ and 45° up to 90° induces adsorption and desorption respectively; while pulling angles between θ^s up to 45° can induce *both* adsorption and desorption depending on the pulling force. We note that the studied alternate model in [29] that weighted surface visit *sites* yielded analogous behaviour.

In three dimensions, while the order of the transition remains unchanged, the physical analysis of the model reveals that vertical (as well as near vertical) pulling results in critical force–temperature curves that exhibit local maximum at low temperature—referred to as *re-entrance phenomena*. Such phenomena has been justified by low-temperature approximation arguments in [23, 24] and [28] that show that a positive slope in the critical force–temperature curve is due to the non-zero conformational entropy per adsorbed monomer. This re-entrance type phenomenon has not been seen in two-dimensional homo-polymer lattice models.

Alternatively, to capture the effects of stiffness we define a horizontal and vertical *stiffness site* as an internal site in w that lies between two consecutive horizontal and vertical steps respectively. Note that thus a stiffness site cannot occur at the end-points of a walk. Similarly, we attribute each horizontal (vertical) stiffness site with energy gains of $-\Delta_x$ ($-\Delta_y$), so that if w contains ℓ_x horizontal (ℓ_y vertical) stiffness sites then the overall energy change due to horizontal and vertical stiffness is $-\ell_x(w)\Delta_x$ and $-\ell_y(w)\Delta_y$, respectively. Boltzmann weights

$$\sigma_x := \mathrm{e}^{\Delta_x/T} \tag{6}$$

and

$$\sigma_y := \mathrm{e}^{\Delta_y/T} \tag{7}$$

associated with stiffness are hence defined.

The model with surface energy and horizontal stiffness but no pulling was considered in [25], showing that the adsorption transition remains second order when stiffness is added.

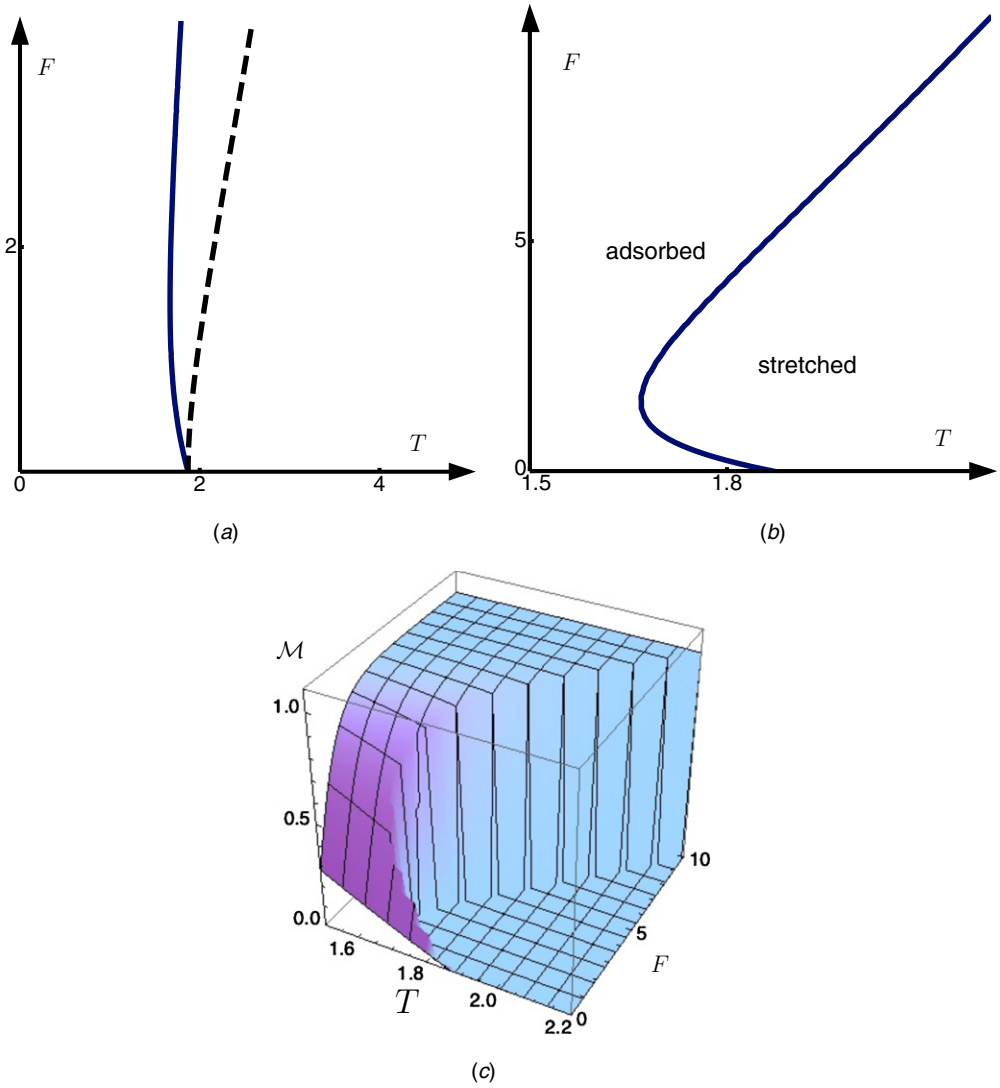

Figure 5. Pulling the polymer at $\theta = 40^\circ$ away from the surface without stiffness. (*a*) The force–temperature critical curve overlaid with the dashed separating angle critical curve. (*b*) A rescaled plot of the critical curve labelled with the phases. (*c*) The order parameter $\mathcal{M}$ in terms of the physical variables T and F.

However, horizontal stiffness does change the location of the critical point. Specifically, an increase in the magnitude of the horizontal stiffness energy $-\Delta_x$, requires a greater critical temperature to induce desorption as is seen in figure 6. Thus, loosely speaking, horizontal stiffness aids the polymer in grafting itself to the attractive surface.

2.2. Our model

We are now in a position to define our generalized adsorption model that incorporates both anisotropic pulling and anisotropic stiffness effects. Specifically, we define the Hamiltonian

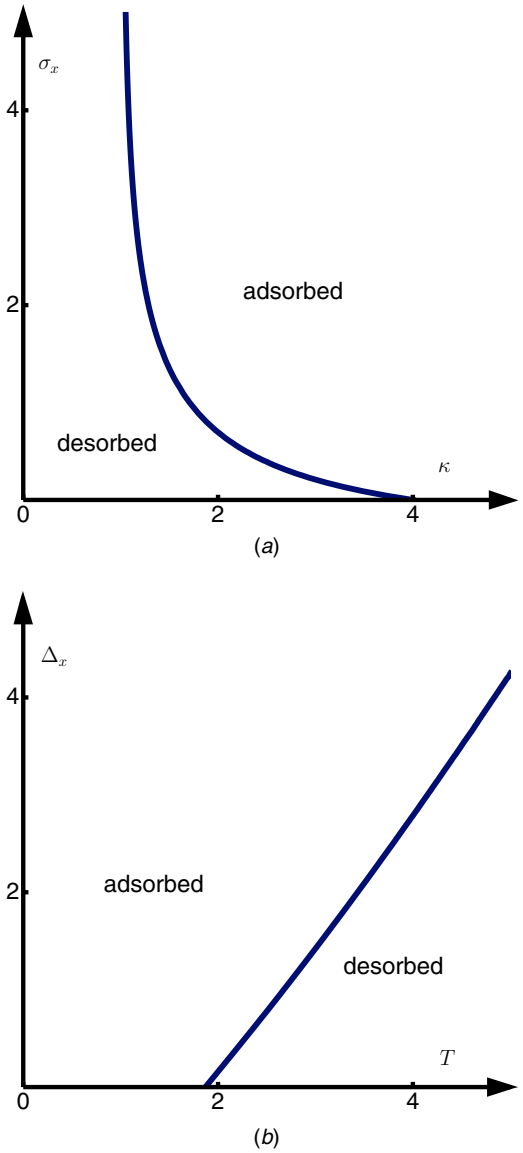

Figure 6. The adsorption model with horizontal stiffness and no pulling: the critical curve for the adsorption phase transition plotted in terms of (*a*) the Boltzmann factors σ_x (horizontal stiffness weight) against κ (surface attraction weight); and in terms of (*b*) the physical variables Δ_x (horizontal stiffness energy) against T (temperature).

$\mathcal{H}$ of the system to be

$$\mathcal{H}(w) = -k(w)J - \ell_x(w)\Delta_x - \ell_y(w)\Delta_x - h_x(w)F\cos\theta - h_y(w)F\sin\theta, \quad w \in \mathcal{W}_L, \tag{8}$$

containing all the energies previously defined. Thus when normalizing the Boltzmann constant k_B to 1, the overall Boltzmann weight for a particular walk w is

$$\begin{aligned} \mathrm{e}^{-\mathcal{H}(w)/T} &= \mathrm{e}^{[k(w)J]/T}\,\mathrm{e}^{[\ell_x(w)\Delta_x]/T}\,\mathrm{e}^{[\ell_y(w)\Delta_y]/T}\,\mathrm{e}^{[h_x(w)F\cos\theta]/T}\,\mathrm{e}^{[h_y(w)F\sin\theta]/T} \\ &= \kappa^{k(w)}\sigma_x{}^{\ell_x(w)}\sigma_y{}^{\ell_y(w)}\mu_x{}^{h_x(w)}\mu_y{}^{h_y(w)}, \end{aligned} \tag{9}$$

where we recall the Boltzmann factors to be defined as

$$\sigma_x := \mathrm{e}^{\Delta_x/T}, \qquad \sigma_y := \mathrm{e}^{\Delta_y/T}, \qquad \mu_x := \mathrm{e}^{F\cos\theta/T}, \qquad \mu_y := \mathrm{e}^{F\sin\theta/T}, \qquad \kappa := \mathrm{e}^{J/T}.$$

An example of the weight attributed to a particular allowed configuration can be seen in figure 1.

Equipped with our Hamiltonian that associates walks in $\mathcal{W}_L$ to Boltzmann weights, we thus define the finite length partition function Z_L as

$$Z_L(\kappa, \sigma_x, \sigma_y, \mu_x, \mu_y) = \sum_{w\in\mathcal{W}_L} \kappa^k {\sigma_x}^{\ell_x} {\sigma_y}^{\ell_y} {\mu_x}^{h_x} {\mu_y}^{h_y} \tag{10}$$

and thus the limiting intensive (reduced) free energy of the system ψ is

$$\psi(\kappa, \sigma_x, \sigma_y, \mu_x, \mu_y) = -\lim_{L\to\infty} \frac{1}{L} \log Z_L(\kappa, \sigma_x, \sigma_y, \mu_x, \mu_y). \tag{11}$$

Next, we first introduce the generating function G defined as

$$G(z; \kappa, \sigma_x, \sigma_y, \mu_x, \mu_y) = \sum_{L\geqslant 1} Z_L(\kappa, \sigma_x, \sigma_y, \mu_x, \mu_y) z^L, \tag{12}$$

where z is conjugate to the walk length L. We note the relation between the free energy ψ and the radius of convergence of G, is given by

$$\psi(\kappa, \sigma_x, \sigma_y, \mu_x, \mu_y) = \log z_c(\kappa, \sigma_x, \sigma_y, \mu_x, \mu_y), \tag{13}$$

where $z_c(\kappa, \sigma_x, \sigma_y, \mu_x, \mu_y)$ is the real and positive singularity of $G(z; \kappa, \sigma_x, \sigma_y, \mu_x, \mu_y)$ with respect to z that is closest to the origin.

Similarly, we again characterize the phases of our system by the order parameters $\mathcal{M}$ and $\mathcal{R}$ defined above, which we can be calculated as

$$\begin{aligned}\mathcal{M}(\kappa, \sigma_x, \sigma_y, \mu_x, \mu_y) &= -\kappa \frac{\partial\, \psi(\kappa, \sigma_x, \sigma_y, \mu_x, \mu_y)}{\partial \kappa} \\ &= -\kappa \frac{\partial \log z_c(\kappa, \sigma_x, \sigma_y, \mu_x, \mu_y)}{\partial \kappa}\end{aligned} \tag{14}$$

and

$$\begin{aligned}\mathcal{R}(\kappa, \sigma_x, \sigma_y, \mu_x, \mu_y) &= -\mu_y \frac{\partial\, \psi(\kappa, \sigma_x, \sigma_y, \mu_x, \mu_y)}{\partial \mu_y} \\ &= -\mu_y \frac{\partial \log z_c(\kappa, \sigma_x, \sigma_y, \mu_x, \mu_y)}{\partial \mu_y}.\end{aligned} \tag{15}$$

2.3. More previously considered cases

An exact solution to the generating function of the model with horizontal stiffness and variable pulling ($\sigma_y = 1$) was found in [26]. It was emphasized there that while horizontal stiffness does not change the order of the phase transition in the model with pulling (first order), it most definitely has an effect on the shape of the critical force–temperature curve, as is seen in figure 7. Specifically, an increase in horizontal stiffness results in a relatively larger (smaller) force required to induce desorption (adsorption) at near vertical (horizontal) pulling angles. We note that no re-entrance was observed.

A model with equal horizontal and vertical stiffness with variable angle pulling was also studied in both two and three dimensions in [10], where once again it was found that the order of the transition remains unchanged as first order. However, more interestingly, an increase in equal horizontal and vertical stiffness still resulted in a greater temperature required to induce desorption as is seen in figure 8, with these effects somewhat dampened

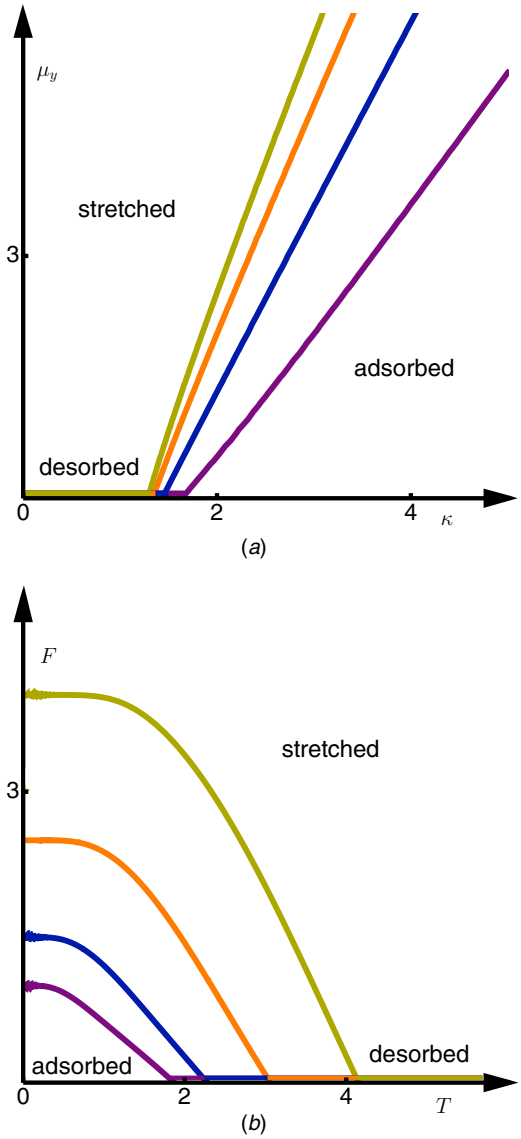

Figure 7. The model with vertical pulling and horizontal stiffness effects: the critical curves plotted in terms of (*a*) Boltzmann factors μ_y against κ for fixed (starting right-most) $\sigma_x = 1.1$, 1.5, 1.8 and 2; and in terms of (*b*) the physical variables F against T for fixed (starting left-most) $\Delta_x = 0$, 0.5, 1.5 and 3.

relative to the horizontal stiffness-only case. Importantly, it was observed that in both two and three dimensions, the zero-temperature critical vertical pulling force required to induce desorption was *independent* of stiffness for $\sigma = \sigma_x = \sigma_y > 1$. In particular, a low-temperature approximation argument highlighted that this zero-temperature critical force is precisely the magnitude of the surface contact energy J. Note, that these results do not hold when the model favours bends in the walk ($\sigma < 1$), whose behaviour at low-temperature was found to be highly dependent on the particular stiffness weight. Again, no re-entrance was observed.

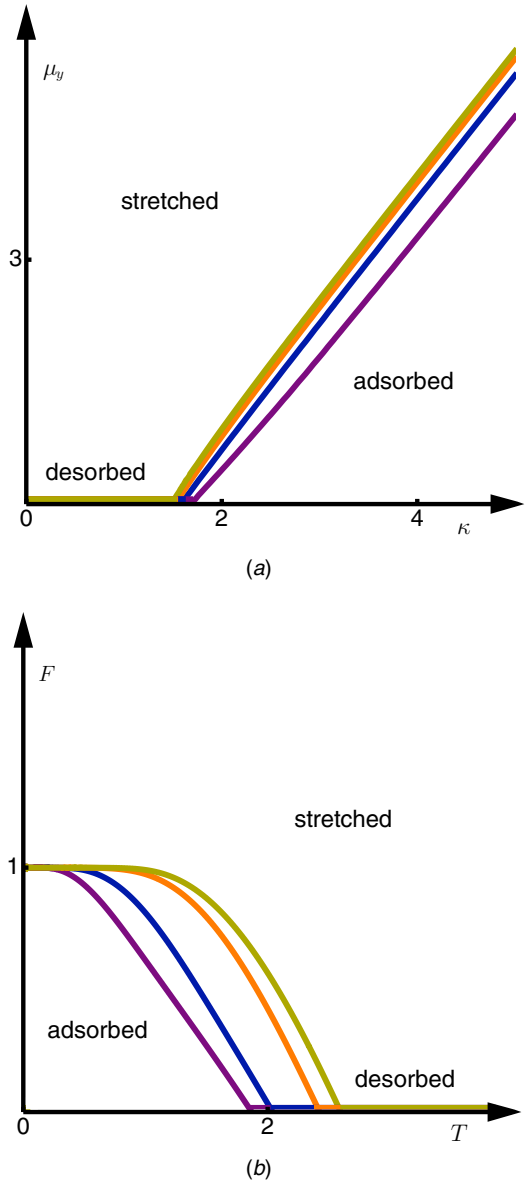

Figure 8. The model with vertical pulling and equal stiffness effects: the critical curves plotted in terms of (*a*) Boltzmann factors μ_y against κ for fixed (starting right-most) $\sigma = 1.1, 1.5, 1.8$ and 2; and in terms of (*b*) the physical variables F against T for fixed (starting left-most) $\Delta = 0, 0.5, 1.5$ and 2.

3. Exact solution of the generating function

Here, we follow the same approach as Osborn and Prellberg [28], who found an exact solution to the generating function of the PDW adsorption model incorporated pulling but without stiffness.

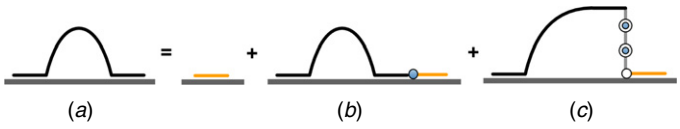

Figure 9. A schematic diagram describing the bijective map that partitions $\mathcal{W}_{\infty,0}$—the class of allowed walks ending at height 0.

Firstly, let $\mathcal{W}_{L,h_y}$ be the subclass of allowable walks $\mathcal{W}_L$ of length L that have final step height h_y. We define the *fixed final height* partition function F_{h_y} as

$$F_{h_y}(y,\kappa,\sigma_x,\sigma_y,\mu_x) = \sum_{L\geqslant 1}\sum_{w\in\mathcal{W}_{L,h_y}} {\mu_x}^{h_x(w)} y^{d_y(w)} \kappa^{k(w)} {\sigma_x}^{\ell_x(w)} {\sigma_y}^{\ell_y(w)}, \tag{16}$$

where y is conjugate to the number of vertical steps in the walk d_y. Thus, the *generalized* generating function F can be defined as

$$F(y,\kappa,\sigma_x,\sigma_y,\mu_x,\mu_y) = \sum_{h_y\geqslant 0} F_{h_y}(y,\kappa,\sigma_x,\sigma_y,\mu_x){\mu_y}^{h_y}. \tag{17}$$

Now, as $L = h_x + d_y$, we can map the generating function G defined at (12) to our generalized generating function F by the simple relation

$$G(z;\kappa,\sigma_x,\sigma_y,\mu_x,\mu_y) = F(z,\kappa,\sigma_x,\sigma_y,z\mu_x,\mu_y) \tag{18}$$

and so it suffices to solve F to find an exact solution to the generating function G.

In solving the generalized generating function F, we will define $F(\mu_y) := F(y,\kappa,\sigma_x,\sigma_y,\mu_x,\mu_y)$, suppressing the first five parameters of the generating function. Moreover, we denote $\mathcal{W}_{\infty,h_y}$ to be the class of allowable walks of *any* length with final step height h_y.

Firstly, we observe that $F(0) \equiv F_0$ which is the fixed final step height partition function restricted to walks that end on the surface. With that in mind, we can establish a functional decomposition for $F(0)$. Recalling that *both* the first and final steps in any allowable walk must be horizontal, we find a suitable bijection from the class of allowable walks of any length ending on the surface $\mathcal{W}_{\infty,0}$ onto itself

$$\mathcal{W}_{\infty,0} \longleftrightarrow \{\,\text{single surface horizontal step}\,\} \tag{19a}$$

$$\bigcup\{\mathcal{W}_{\infty,0}\,\text{adjoined with a surface horizontal step}\,\} \tag{19b}$$

$$\bigcup\{\mathcal{W}_{\infty,h_y\geqslant 1}\,\text{adjoined with h}_\text{y}\,\text{downward vertical steps and a single surface horizontal step}\,\} \tag{19c}$$

which can be visualized schematically in figure 9. Thus, applying our bijection to $F(0)$ we have

$$\begin{aligned} F(0) \equiv F_0 &= \kappa\mu_x \\ &\quad + \kappa\mu_x\sigma_x F_0 \\ &\quad + \kappa\mu_x \sum_{h_y\geqslant 1}\{F_{h_y}\} y^{h_y} {\sigma_y}^{(h_y-1)} \end{aligned} \tag{20}$$

which can be rearranged as

$$\begin{aligned} F(0) &= \kappa \ + \kappa\mu_x\sigma_x F_0 + \frac{\kappa\mu_x}{\sigma_y}\left[\left(\sum_{h_y\geqslant 0}\{F_{h_y}\} y^{h_y}{\sigma_y}^{h_y}\right) - F_0\right] \\ &= \frac{\kappa\mu_x[\sigma_y + F(y\sigma_y)]}{\sigma_y - \kappa\mu_x(\sigma_x\sigma_y - 1)}. \end{aligned} \tag{21}$$

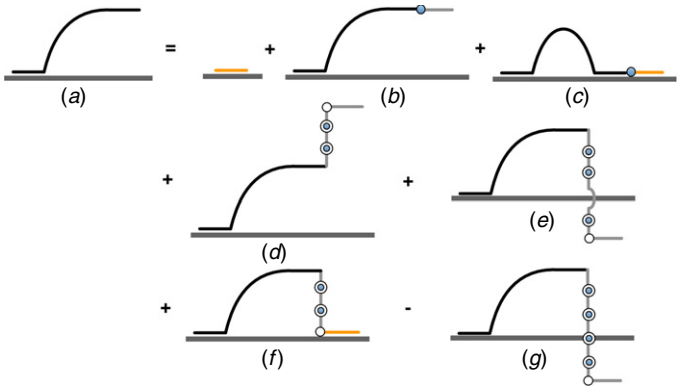

Figure 10. A schematic diagram describing the bijective map that partitions the class of allowed walks ending at *any* height, $\mathcal{W}_{\infty,\infty}$.

By a slightly more complicated construction, we can similarly find a functional decomposition for general $F(\mu)$. For the class of allowable walks of both any length and any final step height $\mathcal{W}_{\infty,\infty} := \cup_{h_y \geqslant 0} \mathcal{W}_{\infty,h_y}$, we have

$$\mathcal{W}_{\infty,\infty} \longleftrightarrow \{\text{single surface horizontal step}\} \tag{22a}$$

$$\bigcup \{\mathcal{W}_{\infty,h_y \geqslant 1} \text{ adjoined with a single horizontal step}\} \tag{22b}$$

$$\bigcup \{\mathcal{W}_{\infty,0} \text{ adjoined with a single surface horizontal step}\} \tag{22c}$$

$$\bigcup \{\mathcal{W}_{\infty,h_y \geqslant 0} \text{ adjoined with } s \geqslant 1 \text{ vertical } \textit{upward} \text{ steps and a single horizontal step}\} \tag{22d}$$

$$\bigcup \{\mathcal{W}_{\infty,h_y \geqslant 1} \text{ adjoined with } s \geqslant 1, \text{s} \neq \text{h vertical } \textit{downward} \text{ steps and a single horizontal step}\} \tag{22e}$$

$$\bigcup \{\mathcal{W}_{\infty,h_y \geqslant 1} \text{ adjoined with } h_y \text{ vertical } \textit{downward} \text{ steps and a single surface horizontal step}\} \tag{22f}$$

$$- \{\mathcal{W}_{\infty,h_y \geqslant 1} \text{ adjoined with } s > \text{h}_\text{y} \text{ vertical } \textit{downward} \text{ steps and a single horizontal step}\}, \tag{22g}$$

which we can similarly see schematically in figure 10. Thus, our functional decomposition for $F(\mu)$ is

$$\begin{aligned} F(\mu_y) = {} & \kappa \mu_x \\ & + \mu_x \sigma_x \sum_{h_y \geqslant 1} \{F_{h_y}\} \mu^{h_y} \\ & + \kappa \mu_x \sigma_x F(0) \\ & + \mu_x \left(\sum_{h_y \geqslant 0} \{F_{h_y}\} \mu^{h_y} \right) \left(\sum_{s \geqslant 1} (\mu y)^s \sigma_y{}^{(s-1)} \right) \\ & + \mu_x \left[\left(\sum_{h_y \geqslant 1} \{F_{h_y}\} \mu^{h_y} \right) \left(\sum_{s \geqslant 1} \left(\frac{y}{\mu} \right)^s \sigma_y{}^{(s-1)} \right) - \left(\sum_{h_y \geqslant 1} \{F_{h_y}\} \mu^{h_y} \left(\frac{y}{\mu} \right)^{h_y} \sigma_y{}^{(h_y-1)} \right) \right] \end{aligned}$$

$$+\kappa\mu_x\left(\sum_{h_y\geqslant 1}\{F_{h_y}\}\mu^{h_y}\left(\frac{y}{\mu}\right)^{h_y}{\sigma_y}^{(h_y-1)}\right)$$
$$-\mu_x\left(\sum_{h_y\geqslant 1}\{F_{h_y}\}\mu^{h_y}\left(\frac{y}{\mu}\right)^{h_y}{\sigma_y}^{h_y}\right)\left(\sum_{s\geqslant 1}\left(\frac{y}{\mu}\right)^{s}{\sigma_y}^{(s-1)}\right). \tag{23}$$

Again, we can rearrange our expression to obtain

$$K(\mu_y)F(\mu_y)=\kappa\mu_x+\left[\frac{\mu_x(\kappa-1)}{\sigma_y}-\frac{\mu_x y}{\mu_y-y\sigma_y}\right]F(y\sigma_y)+\left[\frac{\mu_x(\kappa-1)(\sigma_x\sigma_y-1)}{\sigma_y}\right]F(0) \tag{24}$$

where

$$K(y,\kappa,\sigma_x,\sigma_y,\mu_x;\mu_y)=:K(\mu_y)=\left(1-\mu_x\sigma_x-\frac{\mu_x y\mu_y}{1-y\sigma_y\mu_y}-\frac{\mu_x y}{\mu_y-y\sigma_y}\right). \tag{25}$$

Next, substituting (21) into (24) we obtain

$$K(\mu_y)F(\mu_y)=\kappa\mu_x+\frac{\kappa(\kappa-1){\mu_x}^2(\sigma_x\sigma_y-1)}{(\sigma_y-\kappa\mu_x\sigma_x\sigma_y+\kappa\mu_x)}$$
$$+F(y\sigma_y)\left[\frac{\mu_x(\kappa-1)}{\sigma_y}-\frac{\mu_x y}{\mu_y-y\sigma_y}+\frac{\kappa(\kappa-1){\mu_x}^2(\sigma_x\sigma_y-1)}{\sigma_y\left(\sigma_y-\kappa\mu_x\sigma_x\sigma_y+\kappa\mu_x\right)}\right] \tag{26}$$

which has reduced the number of unknowns in the functional equation down to two—namely, $F(\mu_y)$ and $F(y\sigma_y)$. The motivation for introducing the generalized generating function $F(\mu_y)$ is now apparent as we can solve functional equation (26) by means of the *kernel method*. Specifically, we observe that by choosing an appropriate value for μ_y such that the $K(\mu_y)=0$, we can further eliminate $F(\mu_y)$ from our equation and thus determine $F(y\sigma_y)$ exactly. Note, that we are relying on the fact that $F(y\sigma_y)$ is *independent* of μ_y.

With that in mind, we find $K(\mu_y)$ contains two roots with respect to μ_y. However, only one of these roots is yields a solution to the generating function G that agrees with the combinatorial interpretation of the generating function. We denote such a root as μ_p, where

$$\mu_p(y,\sigma_x,\sigma_y,\mu_x)=\Big[1-\mu_x\sigma_x+y^2{\sigma_y}^2+2\mu_x y^2\sigma_y-\mu_x y^2\sigma_x{\sigma_y}^2$$
$$-\sqrt{\left(1-\mu_x\sigma_x+y^2{\sigma_y}^2+2\mu_x y^2\sigma_y-\mu_x y^2\sigma_x{\sigma_y}^2\right)^2-4(\sigma_y y+\mu_x y-\sigma_x\sigma_y\mu_x y)^2}\Big]$$
$$\times\frac{1}{2[y\sigma_y+\mu_x y(1-\sigma_x\sigma_y)]}. \tag{27}$$

Therefore, setting $\mu_y=\mu_p$ into (26) and solving for $F(y\sigma_y)$ we obtain

$$F(y\sigma_y)=\frac{\kappa(\mu_p-y\sigma_y)[(\mu_x\sigma_x-1)\sigma_y-\mu_x]}{\mu_x+\mu_p(\kappa-1)+\kappa y\sigma_y(\mu_x\sigma_x-1)-y\kappa} \tag{28}$$

and thus substituting (28) into (26) we find the exact solution to the generalized generating function $F(\mu_y)$ to be

$$F(y,\kappa,\sigma_x,\sigma_y,\mu_x,\mu_y)$$
$$=\frac{\mu_x y\kappa(\mu_y-\mu_p)(y\sigma_y\mu_y-1)[\mu_x-\sigma_y(\mu_x\sigma_x-1)]}{[\mu_y-\mu_x\sigma_x\mu_y+y(1+{\mu_y}^2)[-\mu_x+\sigma_y(\mu_x\sigma_x-1)]+y^2\sigma_y\mu_y(\sigma_y+2\mu_x-\mu_x\sigma_x\sigma_y)]}$$
$$\times\frac{1}{(\mu_p(\kappa-1)+y\kappa[-\mu_x+\sigma_y(\mu_x\sigma_x-1)])}. \tag{29}$$

Finally, as we are after the generating function G, we recall relation (18) and thus

$$G(z;\kappa,\sigma_x,\sigma_y,\mu_x,\mu_y) = F(z,\kappa,\sigma_x,\sigma_y,z\mu_x,\mu_y)$$
$$= \frac{\mu_x z^2\kappa(\mu_y-\nu_p)(z\sigma_y\mu_y-1)[\mu_x z-\sigma_y(\mu_x z\sigma_x-1)]}{[\mu_y-\mu_x z\sigma_x\mu_y+z(1+\mu_y{}^2)[-\mu_x z+\sigma_y(\mu_x z\sigma_x-1)]+z^2\sigma_y\mu_y(\sigma_y+2\mu_x z-\mu_x z\sigma_x\sigma_y)]}$$
$$\times\frac{1}{(\nu_p(\kappa-1)+z\kappa[-\mu_x z+\sigma_y(z\sigma_x-1)])}, \tag{30}$$

where

$$\nu_p(z,\sigma_x,\sigma_y,\mu_x) = \mu_p(z,\sigma_x,\sigma_y,z\mu_x)$$
$$= [1-\mu_x z\sigma_x+z^2\sigma_y{}^2+2\mu_x z^3\sigma_y-\mu_x z^3\sigma_x\sigma_y{}^2$$
$$-\sqrt{-4(z\sigma_y+\mu_x z^2-\mu_x z^2\sigma_x\sigma_y)^2+(1-\mu_x z\sigma_x+z^2\sigma_y{}^2+2\mu_x z^3\sigma_y-\mu_x z^3\sigma_x\sigma_y{}^2)^2}]$$
$$\times\frac{1}{2[z\sigma_y+\mu_x z^2(1-\sigma_x\sigma_y)]}. \tag{31}$$

Indeed, expanding our solution to the generating function to attain the first few coefficients yields

$$\begin{aligned} G(z;\kappa,\sigma_x,\sigma_y,\mu_x,\mu_y) = {} & \mu_x\kappa z \\ & + \mu_x{}^2\sigma_x\kappa^2 z^2 \\ & + \mu_x\kappa\left(\mu_x\mu_y+\mu_x{}^2\sigma_x{}^2\kappa^2\right)z^3 \\ & + \mu_x\kappa\left(\mu_x{}^2\mu_y\sigma_x+\mu_x\mu_y{}^2\sigma_y+\mu_x{}^2\mu_y\sigma_x\kappa+\mu_x{}^3\sigma_x{}^3\kappa^3\right)z^4+O(z^5) \end{aligned} \tag{32}$$

as expected.

4. Singularity analysis

We begin by first decomposing the generating function G defined at (30) as a combination of polynomial functions in z. Let

$$A(z;\kappa,\sigma_x,\sigma_y,\mu_x,\mu_y) = \mu_x z^2\kappa(z\sigma_y\mu_y-1)[\mu_x z-\sigma_y(\mu_x z\sigma_x-1)],$$
$$B(z;\sigma_x,\sigma_y,\mu_x,\mu_y) = \mu_y-\mu_x z\sigma_x\mu_y+z(1+\mu_y{}^2)[-\mu_x z+\sigma_y(\mu_x z\sigma_x-1)]$$
$$+z^2\sigma_y\mu_y(\sigma_y+2\mu_x z-\mu_x z\sigma_x\sigma_y),$$
$$C(z;\kappa,\sigma_x,\sigma_y,\mu_x) = z\kappa[-\mu_x z+\sigma_y(z\sigma_x-1)],$$
$$a(z;\sigma_x,\sigma_y,\mu_x) = 1-\mu_x z\sigma_x+z^2\sigma_y{}^2+2\mu_x z^3\sigma_y-\mu_x z^3\sigma_x\sigma_y{}^2,$$
$$b(z;\sigma_x,\sigma_y,\mu_x) = -4(z\sigma_y+\mu_x z^2-\mu_x z^2\sigma_x\sigma_y)^2$$
$$+\left(1-\mu_x z\sigma_x+z^2\sigma_y{}^2+2\mu_x z^3\sigma_y-\mu_x z^3\sigma_x\sigma_y{}^2\right)^2 \quad \text{and}$$
$$d(z;\sigma_x,\sigma_y,\mu_x) = 2[z\sigma_y+\mu_x z^2(1-\sigma_x\sigma_y)], \tag{33}$$

which by inspection of (30) and (31) as well as some algebraic manipulation gives us

$$G(z;\kappa,\sigma_x,\sigma_y,\mu_x,\mu_y) = \frac{A(z)[d(z)\mu_y-(a(z)-\sqrt{b(z)})]}{B(z)[(a(z)-\sqrt{b(z)})(\kappa-1)+d(z)C(z)]}. \tag{34}$$

Here, we find that the generating function G contains a square-root singularity that is given by the smallest root of $b(z;\sigma_x,\sigma_y,\mu_x)$, which corresponds to the system lying in a *desorbed* phase. Thus, we denote this root as $z_d(\sigma_x,\sigma_y,\mu_x)$ where,

$$z_d(\sigma_x,\sigma_y,\mu_x) = \frac{\mu_x\sigma_x+\sigma_y-\sqrt{8\mu_x+\mu_x^2\sigma_x^2-2\mu_x\sigma_x\sigma_y+\sigma_y^2}}{2\mu_x(\sigma_x\sigma_y-2)}. \tag{35}$$

Additionally, we find that G exhibits two simple poles that are determined by the smallest roots of $B(z;\sigma_x,\sigma_y,\mu_x,\mu_y)$ and $D(z;\kappa,\sigma_x,\sigma_y,\mu_x)$, corresponding to the system lying in a *stretched* and *adsorbed* phase respectively, where

$$D(z;\kappa,\sigma_x,\sigma_y,\mu_x) := [a(z)-\sqrt{b(z)}](\kappa-1)+d(z)C(z), \tag{36}$$

and so we denote these roots as $z_s(\sigma_x,\sigma_y,\mu_x,\mu_y)$ and $z_a(\kappa,\sigma_x,\sigma_y,\mu_x)$. Moreover, it is easy to check that when $\mu_y=1$, $z_d(\sigma_x,\sigma_y,\mu_x)$ is also a root of $B(z)$ and that the roots of $B(z)$ are a strict subset to those found in $b(z)$. Thus, in this instance $z_d(\sigma_x,\sigma_y,\mu_x)$ is a *divergent* square root singularity as it is the smallest root of *both* $B(z)$ and $b(z)$. This means that for any restricted model that ignores vertical pulling by setting $\mu_y=1$, we only need to compare $z_d(\sigma_x,\sigma_y,\mu_x)$ with the smallest root of $D(z)$, $z_a(\kappa,\sigma_x,\sigma_y,\mu_x)$, to determine the overall smallest singularity $z_c(\kappa,\sigma_x,\sigma_y,\mu_x,\mu_y)$ of the generating function G. Conversely, when $\mu_y>1$, we find that $z_s<z_d$ and so the competition of finding z_c lies solely between the stretched z_s and adsorbed z_a singularities. Thus, for the purposes of our physical analysis, where we are particularly interested in a non-zero pulling force F at a non-zero pulling angle θ (i.e. $\mu_y>1$), we aim to find the critical surface in terms of F, θ, Δ_x and Δ_y that describes when the stretched and adsorbed singularities coincide.

Now, determining z_s and z_a explicitly is not possible. However, if we are interested in where they become equal, it proves to be fruitful to firstly express the solution to $D(z;\kappa,\sigma_x,\sigma_y,\mu_x)=0$ implicitly in terms of κ, which we denote as $\kappa=\kappa_a(z_a;\sigma_x,\sigma_y,\mu_x)$, where

$$\kappa_a(z;\sigma_x,\sigma_y,\mu_x)=\frac{n(z)-\sqrt{n(z)^2-4m(z)^2}}{n(z)-2m(z)^2-\sqrt{n(z)^2-4m(z)^2}} \tag{37}$$

with

$$\begin{aligned} n(z) &:= n(z,\mu_x,\sigma_x,\sigma_y) = 1-\mu_x\sigma_x z+\sigma_y^2 z^2+\left(2\mu_x\sigma_y-\mu_x\sigma_x\sigma_y^2\right)z^3 \\ m(z) &:= m(z,\mu_x,\sigma_x,\sigma_y) = \sigma_y z+(1-\sigma_x\sigma_y)\mu_x z^2, \end{aligned} \tag{38}$$

and secondly similarly express the solution of $B(z;\kappa,\sigma_x,\sigma_y,\mu_x,\mu_y)=0$ implicitly in terms of μ_y as $\mu_y=\mu_s(z_s;\sigma_x,\sigma_y,\mu_x)$ where

$$\mu_s(z;\sigma_x,\sigma_y,\mu_x)=\frac{n(z)+\sqrt{n(z)^2-4m(z)^2}}{2m(z)}. \tag{39}$$

Considering first (37) we have

$$\begin{aligned} \frac{1}{\kappa_a(z)} &= 1-\frac{2m(z)}{n(z)-\sqrt{n(z)^2-4m(z)^2}} \\ &\Rightarrow \frac{\kappa_a(z)}{1-\kappa_a(z)}\,m(z)=\frac{n(z)-\sqrt{n(z)^2-4m(z)^2}}{2m(z)} \end{aligned} \tag{40}$$

and thus multiplying (39) with (40) we get

$$\begin{aligned} \mu_s(z)\times\frac{\kappa_a(z)}{1-\kappa_a(z)}\,m(z) &= \left[\frac{n(z)+\sqrt{n(z)^2-4m(z)^2}}{2m(z)}\right]\times\left[\frac{n(z)-\sqrt{n(z)^2-4m(z)^2}}{2m(z)}\right] \\ &= \frac{n(z)^2-n(z)^2+2m(z)}{2m(z)} \\ &= 1. \end{aligned} \tag{41}$$

Solving (41) for z gives us two solutions, with the unique combinatorially relevant solution denoted as $z_{s=a}(\kappa, \sigma_x, \sigma_y, \mu_x, \mu_y)$ being

$$z_{s=a}(\kappa, \sigma_x, \sigma_y, \mu_x, \mu_y) = \frac{\kappa\mu_y\sigma_y - \sqrt{\kappa^2\mu_y{}^2\sigma_y^2 - 4(-1+\kappa)(-\kappa\mu_x\mu_y + \kappa\mu_x\mu_y\sigma_x\sigma_y)}}{2(-\kappa\mu_x\mu_y + \kappa\mu_x\mu_y\sigma_x\sigma_y)} \tag{42}$$

and thus finally our critical surface can be defined as a function of μ_y by substituting (42) into (39) to get

$$\begin{aligned}\mu_{s=a}(\sigma_x, \sigma_y, \mu_x) &:= \mu_s(z_{s=a}; \sigma_x, \sigma_y, \mu_x) \\ &= \frac{n(z_{s=a}, \mu_x, \sigma_x, \sigma_y) + \sqrt{n(z_{s=a}, \mu_x, \sigma_x, \sigma_y)^2 - 4m(z_{s=a}, \mu_x, \sigma_x, \sigma_y)^2}}{2m(z_{s=a}, \mu_x, \sigma_x, \sigma_y)}.\end{aligned} \tag{43}$$

which is a function expressed solely in terms μ_x, σ_x and σ_y. Recall, that these factors are themselves defined solely in terms of the physical variables and so we have indeed reached our objective of describing the critical surface only in terms of T, F and θ (as well as the stiffness energy variables).

5. Phase transitions of the general stiffness model

To describe our general stiffness model we introduce a 'stiffness ratio' $r \in [0, 1]$ and stiffness strength Δ, with the latter variable partitioned into its respective horizontal and vertical components so that

$$\Delta_x \equiv (1-r)\Delta \text{ and equivalently } \sigma_x \equiv \sigma^{(1-r)} \tag{44}$$

and

$$\Delta_y \equiv r\Delta \text{ and equivalently } \sigma_y \equiv \sigma^r, \tag{45}$$

respectively. We now proceed to show that both without and with pulling, the order of the adsorption phase transition remains unaffected for *any* stiffness ratio $0 \leqslant r \leqslant 1$.

5.1. Phase transitions without pulling: $0 \leqslant r \leqslant 1$, $\mu_y = \mu_x = 1$

Looking first at when $\mu_y = \mu_x = 1$, we perform our parameter substitution into (35), where the desorbed singularity becomes

$$z_d(\sigma, r) = \frac{\sigma^{-r}(\sigma^{2r} + \sigma - \sqrt{\sigma^{4r} - 2(-4+\sigma)\sigma^{2r} + \sigma^2})}{2(-2+\sigma)} \tag{46}$$

while our implicit solution to the adsorbed root z_a (37) is

$$\kappa_a(z; \sigma, r) = \frac{n(z) - \sqrt{n(z)^2 - 4m(z)^2}}{n(z) - 2m(z)^2 - \sqrt{n(z)^2 - 4m(z)^2}}, \tag{47}$$

where

$$\begin{aligned} n(z) &:= n(z, \sigma, r) = 1 + z^2\sigma^{2r} - z\sigma^{1-r} + 2z^3\sigma^r - z^3\sigma^{1+r}, \\ m(z) &:= m(z, \sigma, r) = z\sigma^r + z^2 - z^2\sigma. \end{aligned} \tag{48}$$

Thus, both singularities (46) and (47) coincide when $\kappa_{a=d}(\sigma, r) := \kappa_a(z_d; \sigma, r)$.

Now, fixing $0 \leqslant r \leqslant 1$, it can be shown that for any $\sigma \geqslant 1$, $\kappa_a(z; \sigma, r)$ is a strictly *decreasing* function of z in the region $0 < z < z_d(\sigma, r)$. This means that for $\kappa > \kappa_{a=d}(\sigma, r)$,

$z_a(\kappa, \sigma, r)$ is smaller than $z_d(\sigma, r)$ and so we can finally describe the overall smallest singularity $z_c(\kappa, \sigma, r)$ as

$$z_c(\kappa, \sigma, r) = \begin{cases} z_d(\sigma, r) & \kappa \leqslant \kappa_{a=d}(\sigma, r) \\ z_a(\kappa, \sigma, r) & \kappa > \kappa_{a=d}(\sigma, r) \end{cases} \tag{49}$$

and we are now in a position to find the average fraction of adsorbed steps $\mathcal{M}$. Recalling the description for the order parameter at (14) we observe that as $z_d(\sigma, r)$ is independent of κ, $\mathcal{M} = 0$ when $\kappa \leqslant \kappa_{a=d}(\sigma, r)$.

Now for the case where $\kappa > \kappa_{a=d}(\sigma, r)$, as we do not know $z_a(\kappa, \sigma, r)$ explicitly, we instead aim to describe the asymptotic behaviour of $\mathcal{M}$ near the critical point z_d as $z \uparrow z_d$ and thus $\kappa \downarrow \kappa_a$. Firstly, expanding our implicit function $D(\kappa, \sigma, r) = 0$ defined at (58) around the point $z = z_d$, we have

$$\kappa_a(z; \sigma, r) \approx \frac{n(z_d; \sigma, r) + c_1(z; \sigma, r)\sqrt{z_d - z}}{n(z_d; \sigma, r) - 2m(z_d; \sigma, r)^2 + O(z_d - z)^{1/2}}, \quad z \uparrow z_d, \tag{50}$$

where $c_1(z; \sigma, r)$ is a non-zero algebraic function of z, σ and r. Moreover, as

$$\kappa_{a=d}(\sigma, r) = \frac{n(z_d; \sigma, r)}{n(z_d; \sigma, r) - 2m(z_d; \sigma, r)^2} \tag{51}$$

we can simplify (50) to become

$$\kappa_a(z; \sigma, r) - \kappa_{a=d}(\sigma, r) \approx c_1(z; \sigma, r)\sqrt{z_d - z}, \quad z \uparrow z_d \tag{52}$$

and thus solving for z we can describe the behaviour of $z_a(\kappa, \sigma, r) \uparrow z_d(\sigma, r)$ as $\kappa \downarrow \kappa_{a=d}(\sigma, r)$

$$z = z_a \approx z_d - \frac{1}{c_1(z; \sigma, r)^2}[\kappa_a(z; \sigma, r) - \kappa_{a=d}(\sigma, r)]^2 \tag{53}$$

which allows us to conclude that

$$\lim_{\kappa \downarrow \kappa_{a=d}(\sigma, r)} \mathcal{M}(\kappa, \sigma, r) = -\kappa \left(\frac{\partial \log z_a}{\partial z_a} \times \frac{\partial z_a}{\partial \kappa} \right) = 0. \tag{54}$$

Therefore, $\mathcal{M}$ is continuous around the critical point and so we do not observe a first-order phase transition. However, when we consider the first derivative of $\mathcal{M}$ with respect to κ as $\kappa \downarrow \kappa_{a=d}(\sigma, r)$ we find

$$\lim_{\kappa \downarrow \kappa_{a=d}(\sigma, r)} \frac{\partial \mathcal{M}(\kappa, \sigma, r)}{\partial \kappa} = -\kappa \left(\frac{\partial^2 \log z_a}{\partial {z_a}^2} \times \frac{\partial^2 z_a}{\partial \kappa^2} \right) = c_2(z, \mu_x, r) \tag{55}$$

where again $c_2(z, \mu_x, r)$ is a non-zero algebraic function of z, σ and r. Thus,

$$\frac{\partial \mathcal{M}(\kappa, \sigma, r)}{\partial \kappa} = \begin{cases} 0 & \kappa \leqslant \kappa_{a=d}(\sigma, r) \\ c_2(z, \sigma, r) & \kappa > \kappa_{a=d}(\sigma, r) \end{cases} \tag{56}$$

implying that we have a finite-jump discontinuity at the critical point. Moreover, as $\partial \mathcal{M}/\partial \kappa$ is a second derivative with respect to the free energy, we conclude that the general stiffness model with no pulling exhibits a second-order phase transition for *any* stiffness ratio $0 \leqslant r \leqslant 1$. Indeed, figure 11, plotting $\mathcal{M}$ against κ for a range of different stiffness ratios displays our conclusion. Here, we observe that as r increases, $\kappa_{a=d}$ also increases, as a larger weight placed on vertical stiffness sites implies that a greater surface contact weight κ is required to induce adsorption. Finally, note that as we are ignoring vertical pulling, our second order parameter $\mathcal{R}$, which we recall is a first derivative with respect to μ_y, is thus in this instance 0 over the entire considered domain.

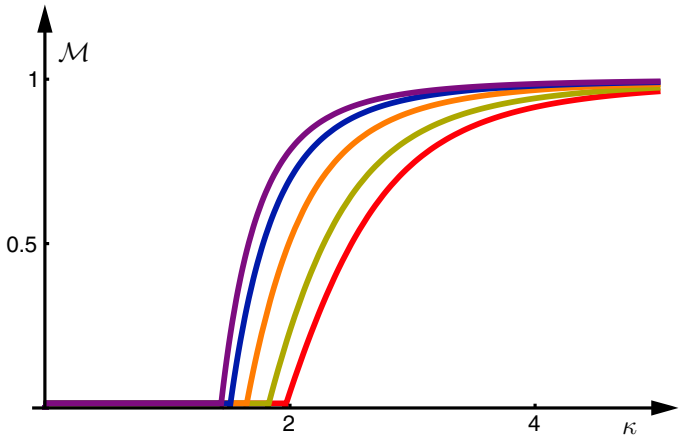

Figure 11. The general stiffness model with no pulling: $\mathcal{M}$ against κ for fixed $\sigma = 1.5$. The stiffness ratios, starting from the left-most (purple) curve and moving right are $r = 0, 0.2, 0.5, 0.8$ and 1. For each considered stiffness ratio, the order parameter is continuous but not differentiable at the critical point and so we observe a second-order adsorption phase transition.

5.2. Phase transitions of a general stiffness model with pulling: $0 \leqslant r \leqslant 1$, $\mu_x > 1$ *and* $\mu_y > 1$

We now additionally incorporate the effects of both horizontal and vertical pulling by letting $\mu_x > 1$ and $\mu_y > 1$ respectively. Here, the desorbed singularity z_d defined at (35), which is independent of μ_y, becomes

$$z_d(\sigma, \mu_x, r) = \frac{\sigma^{-r}\left(\sigma^{2r} + \sigma\mu_x - \sqrt{\sigma^{4r} - 2(-4+\sigma)\sigma^{2r}\mu_x + \sigma^2\mu_x^2}\right)}{2(-2+\sigma)\mu_x}, \tag{57}$$

with our implicit solution to the adsorbed root z_a with respect to κ is

$$\kappa_a(z; \sigma, \mu_x, r) = \frac{n(z) - \sqrt{n(z)^2 - 4m(z)^2}}{n(z) - 2m(z)^2 - \sqrt{n(z)^2 - 4m(z)^2}}, \tag{58}$$

and finally the solution to the stretched singularity z_s with respect to μ_y is

$$\mu_s(z; \sigma, \mu_x, r) = \frac{n(z) + \sqrt{n(z)^2 - 4m(z)^2}}{2m(z)}, \tag{59}$$

where

$$\begin{aligned} n(z) &:= n(z, \sigma, \mu_x, r) = \sigma^r + z^2\sigma^{3r} - z\sigma\mu_x - z^3(-2+\sigma)\sigma^{2r}\mu_x, \\ m(z) &:= m(z, \sigma, \mu_x, r) = z\sigma^r(\sigma^r + (z - z\sigma)\mu_x). \end{aligned} \tag{60}$$

Again, one can similarly show that $\forall \mu_y > 1$ and fixed $0 \leqslant r \leqslant 1$, μ_s is a decreasing function of z, implying that $z_s < z_d$. Thus, as we have previously established in section 5.1 that κ_a is a decreasing function of z and moreover that $z_s(\sigma, \mu_x, \mu_y)$ is independent of κ, then that implies that the closest real and positive singularity $z_c(\kappa, \sigma, \mu_x, \mu_y, r)$ is given by

$$z_c(\kappa, \sigma, \mu_x, \mu_y, r) = \begin{cases} z_s(\sigma, \mu_x, \mu_y, r), & \kappa \leqslant \kappa_{a=s}(\sigma, \mu_x, r) \\ z_a(\kappa, \sigma, \mu_x, r), & \kappa > \kappa_{a=s}(\sigma, \mu_x, r) \end{cases} \tag{61}$$

with $\kappa_{a=s}(\sigma, \mu_x, r) := \kappa_a(z_s; \sigma_x, \mu_x, r)$. Considering the order parameter $\mathcal{M}$, we observe that as $z_s(\sigma, \mu_x, \mu_y, r)$, is independent of κ, we have $\mathcal{M} = 0 \forall \kappa \leqslant \kappa_{a=s}(\sigma, \mu_x, r)$. Moreover, as

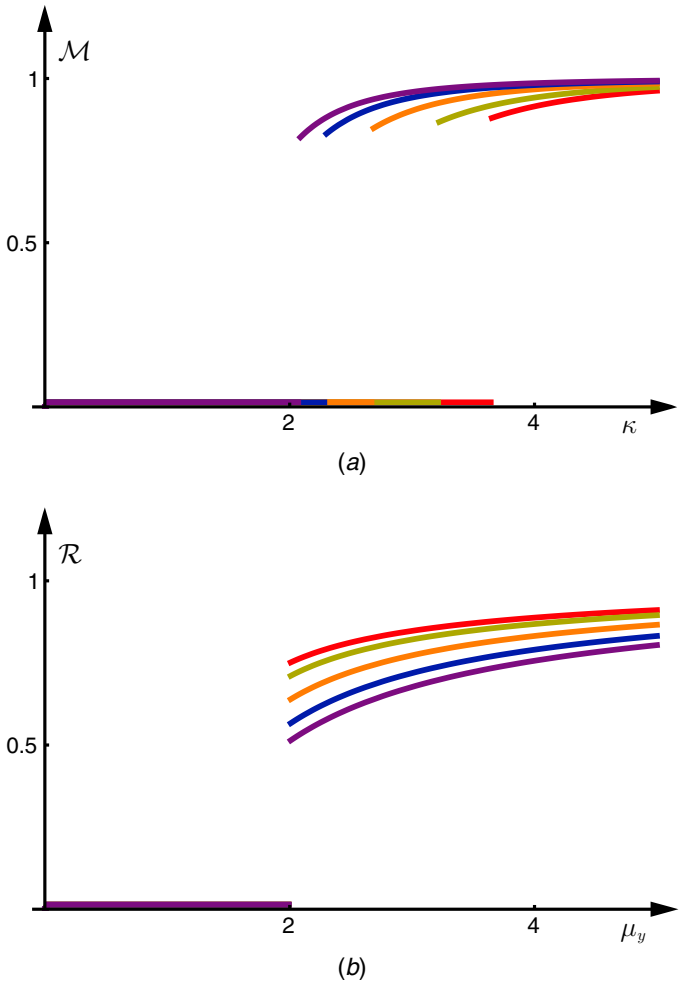

Figure 12. The general stiffness model with both horizontal and vertical pulling: (*a*) $\mathcal{M}$ against κ and (*b*) $\mathcal{R}$ against μ_y for fixed $\sigma = 1.5$, $\mu_x = 1$ over a range of different ratios r. Specifically, the stiffness ratios, starting from the (*a*) left-most (purple) curve and moving right as well as (*b*) bottom-most (purple) curve and moving upward are $r = 0, 0.2, 0.5, 0.8$ and 1. For each r, both order parameters exhibit a finite-jump discontinuity at the critical point $\kappa_{a=s}$ and $\mu_{a=s}$ when fixing μ_y and κ respectively. Thus, we observe a first-order adsorption phase transition.

the singularity $z_a(\kappa, \sigma, \mu_x, r)$ is independent of μ_y, the functional behaviour of $\mathcal{M}$ remains unchanged over the region $\kappa > \kappa_{a=s}(\sigma, \mu_x, r)$ relative to the no pulling case. Thus, the desorbed region where $\mathcal{M} = 0$ has now increased from $0 < \kappa \leqslant \kappa_{a=d}(\sigma, \mu_x, r)$ to $0 < \kappa \leqslant \kappa_{a=s}(\sigma, \mu_x, r)$; while the adsorbed region where $\mathcal{M}$ is non-zero has conversely decreased from $\kappa > \kappa_{a=d}(\sigma, \mu_x, r)$ to $\kappa > \kappa_{a=s}(\sigma, \mu_x, r)$. Moreover, we find that for $\kappa > \kappa_{a=d}(\sigma, \mu_x)$ $(z < z_d)$ and fixed $0 \leqslant r \leqslant 1$, $\mathcal{M}$ is non-zero and thus exhibits a finite-jump discontinuity at the critical point $\kappa_{a=s}(\sigma, \mu_x, r)$ as can be seen in figure 12(*a*). In fact, our inclusion of the secondary order parameter $\mathcal{R}$ described at (15) helps to easily distinguish between a first and second order adsorption phase transition, as we should now expect $\mathcal{R}$ to be non-zero for values of $\kappa \leqslant \kappa_{a=s}(\sigma, \mu_x, r)$. Indeed, by use of the implicit expression μ_s at (59) for the stretched singularity z_s, an almost identical approach employed

in finding $\mathcal{M}$ shows that additionally, the limiting average ratio of final step height to polymer length $\mathcal{R}(\kappa, \sigma, \mu_x, \mu_y, r)$ exhibits a positive finite-jump discontinuity at the critical point as is observed in figure 12(*b*). Thus, overall, we conclude that for any stiffness ratio $0 \leqslant r \leqslant 1$, the system is in an *adsorbed phase* when $\kappa > \kappa_{a=s}$ as $\mathcal{M} > 0, \mathcal{R} = 0$; while we observe a *stretched* phase when $\kappa \leqslant \kappa_{a=s}$ as $\mathcal{M} = 0, \mathcal{R} > 0$.

6. Phase diagrams and physical analysis

6.1. Introduction

In section 5, we introduced the general stiffness model with a stiffness ratio r ranging from $r = 0$ (horizontal-only stiffness) up to $r = 1$ (vertical-only stiffness), finding that the order of the adsorption phase transition is consistent for all ratios $0 \leqslant r \leqslant 1$. We now proceed to analyse this model with respect to its physical variables, and show that in this regard, the model's behaviour is dependent on the stiffness ratio. Specifically, we will be particularly interested in the critical behaviour of the general stiffness model for a non-zero pulling force away from the surface (i.e. $F > 0$). From section 4, we know that this translates into considering the critical surface $\mu_{s=a}$ (43) that describes when both the adsorbed z_a and stretched z_s dominant singularities coincide as a function of F, T, θ as well as the stiffness variables Δ_x and Δ_y. Thus, with respect to the general stiffness model, the critical surface is expressed as

$$\begin{aligned}\mu_{s=a}(\sigma, \mu_x, r) &:= \mu_s(z_{s=a}; \sigma, \mu_x, r) \\ &= \frac{n(z_{s=a}) + \sqrt{n(z_{s=a})^2 - 4m(z_{s=a})^2}}{2m(z_{s=a})}\end{aligned} \tag{62}$$

with $n(z) := n(z, \sigma, \mu_x, r)$ and $m(z) := m(z, \sigma, \mu_x, r)$ expressed in (60), while the point where the adsorbed and stretched singularities coincide becomes

$$z_{s=a}(\kappa, \sigma, \mu_x, \mu_y, r) = \frac{2(\kappa - 1)}{\kappa, \sigma^r \mu_y + \sqrt{\kappa \mu_y [\kappa, \sigma^{2r} \mu_y - 4\mu_x(\kappa - 1)(\sigma - 1)]}}. \tag{63}$$

6.2. Equal horizontal and vertical stiffness with pulling: $r = 0.5$, variable θ

We first look at the previously considered case, described in section 2, and considered in [10], where the model places equal weight on both a horizontal and vertical stiffness site ($\sigma_x = \sigma_y = \sigma > 1$, $\Delta_x = \Delta_y = \Delta > 0$, i.e. $r = 0.5$). Here we explore further the analysis in terms of the model's physical variables for a non-zero pulling force. Substituting $r = 0.5$ into (62) we find an expression for the equal stiffness critical surface that describes when both the stretched and adsorbed dominant singularities coincide. Now, one approach to visualize this surface can be attained by fixing both $-\Delta$ and θ, giving us a curve in T and F. Specifically, in figure 13, for each fixed $\Delta = 0.2, 1, 2$ and 3, we overlay these *force–temperature critical curves* at fixed $\theta = 0^\circ, 15^\circ, 30^\circ, 45^\circ, 60^\circ, 75^\circ, 90^\circ$ on the same plot, allowing us to describe how both the stiffness and the pulling angle individually affect the adsorption transition.

Looking at figure 13, we immediately observe that for each considered case (*a*)–(*d*), all critical-curves intersect when there is no pulling force. This is unsurprising, as the location of the phase transition should be independent of the pulling angle when force is zero. Moreover, by recalling our singularity analysis for the general stiffness case with no pulling in section 5.1, we can express the location of the zero-force adsorption phase transition implicitly in terms of T, denoted as T^c_Δ, to be

$$\mathrm{e}^{1/T^c_\Delta} = \frac{1}{2}\left[3 + \frac{1 - \sqrt{2}\sinh\left(\Delta/T^c_\Delta\right)}{1 + \sqrt{2}\cosh\left(\Delta/T^c_\Delta\right)}\right]. \tag{64}$$

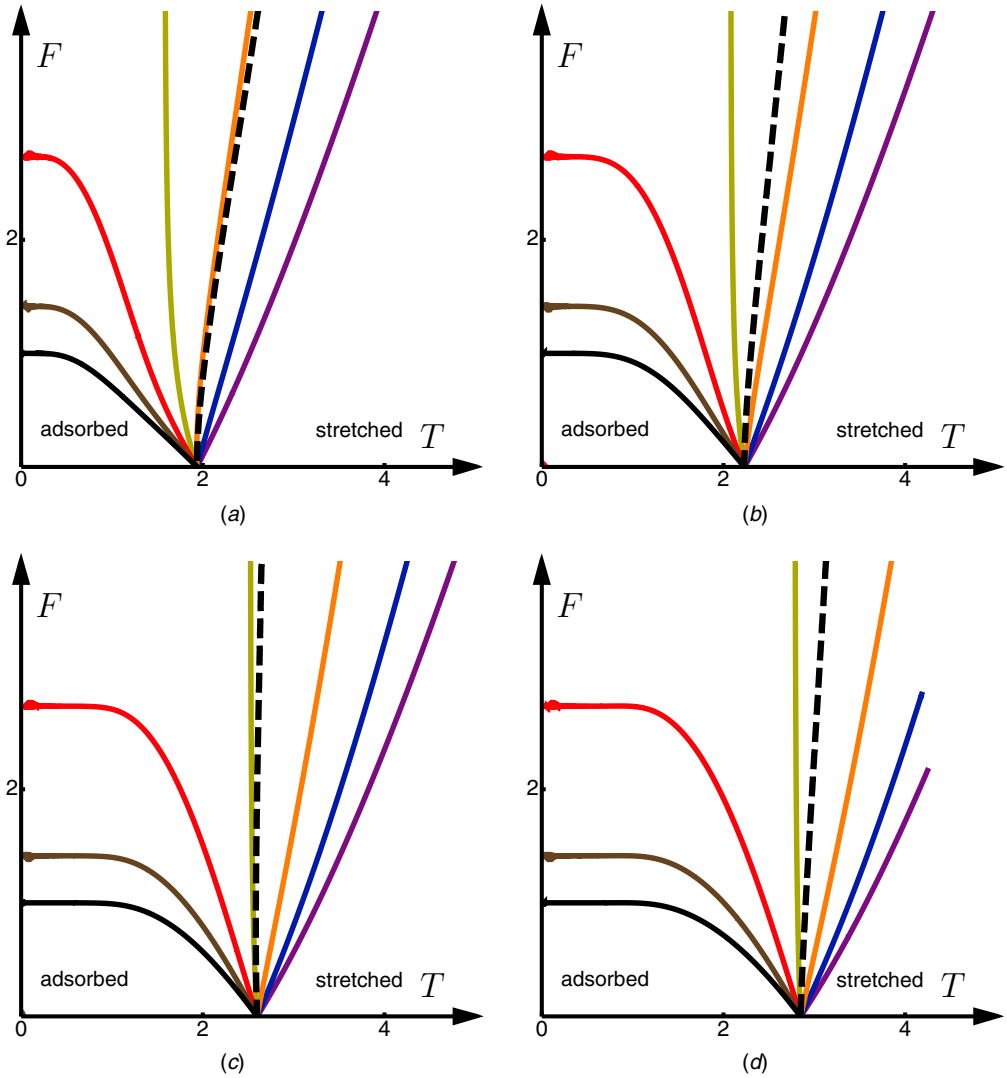

Figure 13. The general stiffness model with $r = 0.5$ (equal stiffness) and both horizontal and vertical pulling: The force–temperature critical curve at different upward pulling angles with the stiffness attractive energy Δ fixed at (*a*) 0.2, (*b*) 1, (*c*) 2 and (*d*) 3. For each plot, starting from the right-most (purple) curve, the individual curves corresponding to an upward pulling angle of $0^\circ, 15^\circ, 30^\circ, 45^\circ, 60^\circ, 75^\circ$ and 90° away from the surface respectively. Additionally, the dashed critical curve corresponds to pulling a polymer at the separating angle.

In particular, we find (a) $T^c_{\Delta=0.2} \approx 1.9359$, (b) $T^c_{\Delta=1} \approx 2.2262$, (c) $T^c_{\Delta=2} \approx 2.6123$ and (d) $T^c_{\Delta=3} \approx 2.9985$. Recall, that for $T < T^c_\Delta$ our model is in an adsorbed phase, while for $T > T^c_\Delta$ we are conversely in a desorbed phase. Thus, from our examples in figure 13, we observe than an increase in Δ results in a higher temperature required to move from an adsorbed to a desorbed phase.

Understanding the zero-force case, we are now in a position to interpret the critical curves when there is a positive upward pulling force. Recall in our review in section 2 that a separating pulling angle $\theta^s_{\Delta=0} \approx 26.6^\circ$ was found for the model with stretching but no stiffness effects, resulting in a critical force–temperature curve that exhibited an infinite slope at zero

force. Moreover, we established that a critical curve that lies immediately to the right of the separating angle curve describes the force required to *definitely* induce *adsorption* for a given temperature T. Here, for the examples in figure 13 we find the separating angles to be (a) $\theta^s_{\Delta=0.2} \approx 28.5765^\circ$, (b) $\theta^s_{\Delta=1} \approx 35.9909^\circ$, (c) $\theta^s_{\Delta=2} \approx 43.4819^\circ$ and (d) $\theta^s_{\Delta=3} \approx 40.8728^\circ$ as seen in figure 13. Therefore, we observe for cases (a) up to (c), that an increase in stiffness *increases* the separating angle, thereby extending the range of pulling angles from 0° to θ^s_Δ which will definitely induce *adsorption* given enough force. However, this trend does not continue for all stiffness values, as we instead observe a *decrease* in the separating angle from $\Delta = 2$ to $\Delta = 3$, implying the existence of an angle $\theta^s_{\max}$ that is a maximum for all stiffness $\Delta \geqslant 0$. In fact, we find that $\theta^s_{\max} = 45^\circ$ when $\Delta \approx 2.239\,44$. Thus, a pulling force whose vertical component is larger than its horizontal counterpart can *never* induce adsorption irrespective of the level of stiffness. Moreover, as per the model with no stiffness introduced in section 2, we again claim that the slope of the force–temperature critical curve corresponding to a pulling angle of 45° must be vertical for large F as the inclusion of equal stiffness simply aids surface contacts in counter-balancing entropic effects at the critical point. Thus, eventually, the location of the transition point as we increase force at a pulling angle, which consists of an *equal* horizontal and vertical component, should not be dependent on temperature. Given this similar behaviour in the critical curve with a corresponding pulling angle of 45°, we again also find that curves with a pulling range between θ^s_Δ up to 45° can induce *both* desorption and adsorption for low and high pulling forces respectively. More interestingly, we find that as $\Delta \to \infty$, $\theta^s_\Delta \to 0^\circ$, implying that as we increase stiffness, a larger range of pulling angles can induce both desorption and adsorption. While such behaviour may seem counter-intuitive, it's important to stress that pulling a polymer at these predominantly horizontal angles only induces desorption within a relatively small range of pulling forces, with such a range moreover decreasing as we increase stiffness. Indeed, we can see this more clearly in figure 14 by plotting critical curves at a fixed pulling angle of $\theta = 43^\circ$ over a range of different stiffness values. Here, starting from the left-most critical curves in figure 14(*a*) that correspond to a stiffness Δ of 0.2 and 1 respectively, we observe that both curves can induce both desorption and adsorption, agreeing with our findings for the separating angle. For the third and fourth leftmost critical curves that correspond to $\Delta = 2$ and 3 respectively, as $\theta^s_{\Delta=2} \approx 43.4819^\circ$ and $\theta^s_{\Delta=3} \approx 40.8728^\circ$, we should observe a shift from a critical curve that induces *only* adsorption to a curve that induces both adsorption and desorption. By re-plotting our curves over a smaller temperature region in figure 14(*b*), we can in fact observe precisely this behaviour. Thus, comparing $\Delta = 2$ and 3, there is an *increase* in the critical force–temperature stretched region. However, we note that for the critical curve corresponding to a stiffness $\Delta = 3$, that the region that can induce desorption is a small sliver relative to the cases $\Delta = 0.2$ and 1 which further diminishes as we increase stiffness. Thus, while increasing stiffness increases the range of pulling angles that induce both adsorption and desorption, the maximal force that will cause desorption *decreases* between the pulling angles θ^s and 45° for large, increasing Δ.

6.3. Horizontal-only stiffness with pulling: $r = 0$, variable θ

In this instance, we substitute $r = 0$ into (43) to express the horizontal-only stiffness critical surface for a non-zero pulling force. As per the case of equal horizontal and vertical stiffness, we plot the force–temperature critical curves in figure 15 over a range of fixed values for Δ_x and θ. From figure 15, we again observe that an increase in Δ_x increases the location of the critical temperature $T^c_{\Delta_x}$, which translates to an increased temperature region over which the model is in an adsorbed phase; agreeing with [25]. More precisely, we find that the zero-force adsorption

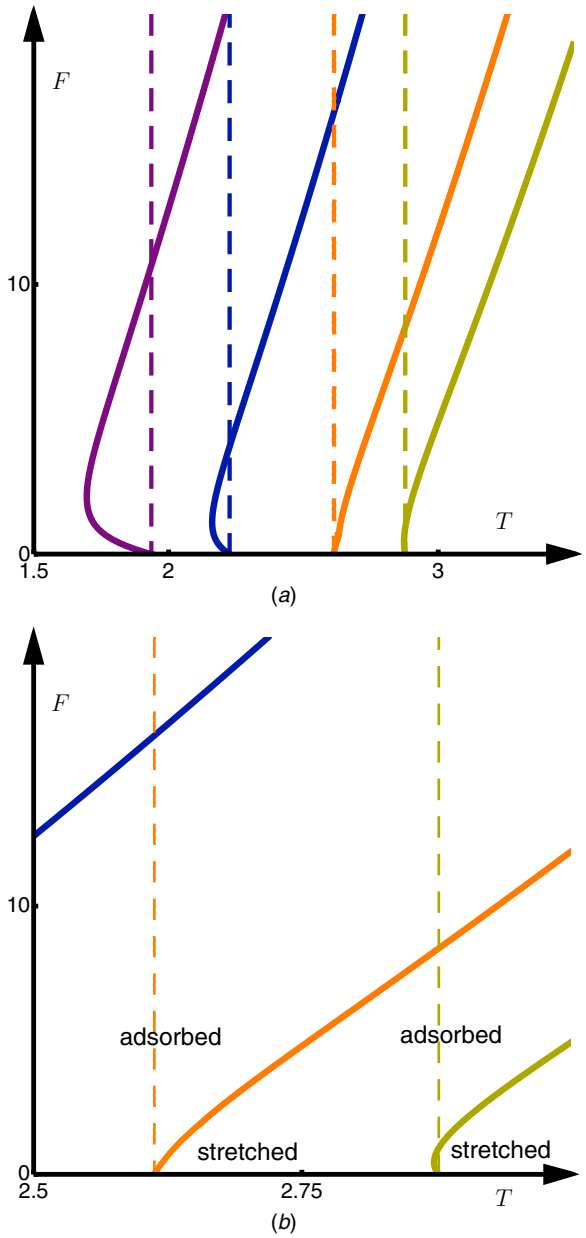

Figure 14. The general stiffness model with $r = 0.5$ (equal stiffness) and both horizontal and vertical pulling: The force–temperature critical curve at a fixed pulling angle of $\theta = 43^\circ$ for a range of different stiffness values. (*a*) Starting from the leftmost (purple) curve, $\Delta = 0.2, 1, 2$ and 3. (*b*) The same plot restricted to the region $2.5 < T < 3$, excluding the critical curve with corresponding stiffness $\Delta_x = 0.2$. Additionally, the corresponding dashed vertical line extends out from the zero-force critical temperature to aid visual inspection of the shape of the critical curve.

transitions occurs at (a) $T^c_{\Delta_x=0.2} \approx 2.033\,86$, (b) $T^c_{\Delta_x=1} \approx 2.674\,48$, (c) $T^c_{\Delta_x=2} \approx 3.432\,26$ and (d) $T^c_{\Delta_x=3} \approx 4.149\,35$. Thus, compared to the case of equal horizontal and vertical stiffness, a greater weight attributed to a (horizontal) stiffness site results in a greater *positive* change in the location of the zero-force critical temperature. Moreover, as per the case of the equal stiffness

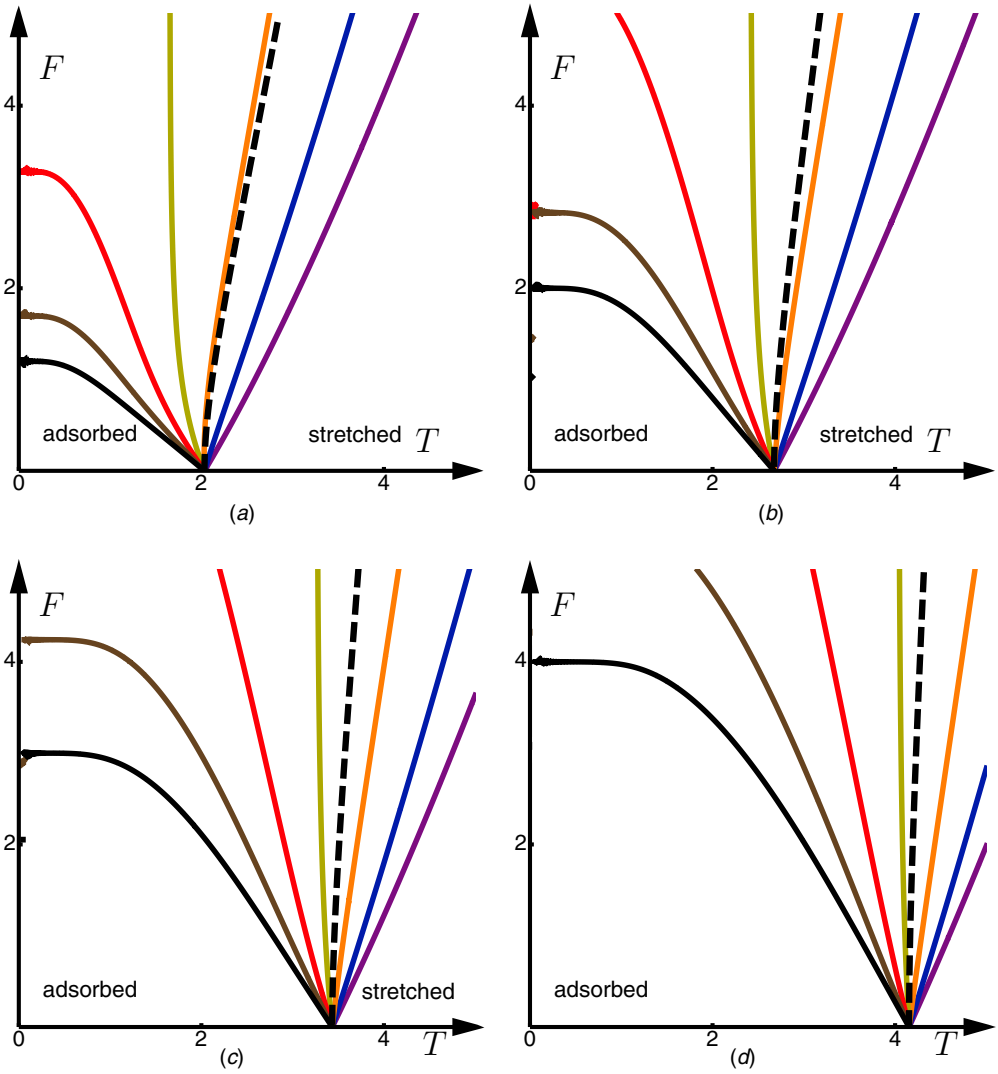

Figure 15. The general stiffness model with $r = 0$ (horizontal-only stiffness) and pulling: The temperature-force critical curves at different upward pulling angles with the stiffness attractive energy Δ_x fixed at (*a*) 0.2, (*b*) 1, (*c*) 2 and (*d*) 3. For each plot, starting from the right-most (purple) curve, the individual curves corresponding to an upward pulling angle of 0°, 15°, 30°, 45°, 60°, 75° and 90° away from the surface respectively. Additionally, the dashed critical curve corresponds to pulling a polymer at the separating angle.

model, we similarly find the separating angle $\theta^s_{\Delta_x}$ for the particular examples in figure 15, which we recall specifies the range of pulling angles from 0° up to $\theta^c_{\Delta_x}$ that definitely induce adsorption given enough force. Recalling that $\theta^c_{\Delta_x=0} \approx 26.6°$, we find (a) $\theta^c_{\Delta_x=0.2} \approx 28.3387°$, (b) $\theta^c_{\Delta_x=1} \approx 33.6499°$, (c) $\theta^c_{\Delta_x=2} \approx 37.741°$ and (d) $\theta^c_{\Delta_x=3} \approx 40.3427°$. Here, for cases (a) to (c) we interestingly observe a *dampened* increase in the separating angle relative to the equal stiffness model. Naively, we might assume the horizontal stiffness model to exhibit a relatively greater positive rate of change in $\theta^s_{\Delta_x}$ as we increase Δ_x, due to the absence of any vertical stiffness. However, by a similar argument as per the case of the equal stiffness model, we

again claim that pulling angles between $\theta^s_{\Delta_x}$ and 45° induce both desorption and adsorption for low and high pulling forces respectively. Thus, as we increase (horizontal) stiffness we see a relatively smaller change in the range of pulling angles that can additionally induce desorption. Moreover, despite observing an increase in the separating angle from (c) to (d) when $\Delta_x = 2$ and $\Delta_x = 3$ respectively, we again find that this trend does not continue for all Δ_x, with a maximal separating angle $\theta^s_{\max} = 45^\circ$ occurring when $\Delta_x \approx 6.760\,76$. Additionally, we similarly find that as $\Delta_x \to \infty$, $\theta^s_{\Delta_x} \to 0^\circ$. Indeed, to display this behaviour, we plot critical curves in figure 16 at a fixed pulling angle of $\theta = 44^\circ$ over a range of stiffness values, with (starting left-most) $\Delta_x = 0.2, 3, 6$ and 8. Here, we do observe an initially increasing separating angle, with the curves corresponding to $\Delta_x = 0.2$ and 3 inducing both adsorption and desorption, while figure 16(*b*) highlights that the separating angle $\theta^s_{\Delta_x=6.0} > 44^\circ$ and thus pulling at such an angle can only shift the system from a desorbed to adsorbed phase. However, a large enough stiffness does result in a decreasing separating angle as seen in figure 16(*c*), where we plot the critical curve corresponding to a stiffness $\Delta_x = 8$ over a restricted temperature domain, showing that once again a pulling force at such an angle can induce either adsorption or desorption. Thus, as per the equal horizontal and vertical stiffness model, eventually, an increase in horizontal stiffness increases the range of pulling angles that can induce both adsorption and desorption. However, as with the case of equal stiffness, the critical force–temperature stretched region does not continue to increase for increasing Δ_x. In fact, while $\theta^s_{\Delta_x}$ does decrease for large stiffness, only an increasingly narrower range of relatively low pulling forces and temperatures are able to induce desorption.

6.4. Vertical-only stiffness: $r = 1$

6.4.1. Vertical-only stiffness and no pulling: $r = 1, F = 0$. The model that incorporates vertical stiffness only ($r = 1$) has not previously been studied within the literature. Thus, we will first consider such a model that ignores pulling ($F = 0$). Now, we have already established in section 5.1, that the general stiffness model with no pulling exhibits a second-order adsorption phase transition for *any* $0 \leqslant r \leqslant 1$. Therefore, we immediately know that the vertical-only stiffness model similarly exhibits a second-order phase transition. Further analysing this sub-case, we plot the phase diagram both in terms of the Boltzmann factors and physical variables in figure 17. Comparing the critical *stiffness–temperature* curve in figure 17(*b*) against the *force–temperature* critical curve in figure 3(*b*) we observe curves that exhibit similar functional behaviour, that are in direct contrast to the observed phase diagram for the case of horizontal only stiffness in figure 6(*b*). Here, an increase in vertical stiffness places a greater weight on polymer configurations with a higher number of consecutive vertical relative to horizontal steps. Even though a stiffer polymer results in less entropy, in this instance, as we increase vertical stiffness, we are more likely to observe configurations consisting of predominantly vertical steps that are normal to the adsorbing surface. Indeed, the system is only adsorbed when both temperature and stiffness strength are low: see figure 17(*b*). At zero temperature there is a phase transition at stiffness strength $\Delta = 1$. Thus, loosely speaking, vertical stiffness affects a polymer more like an upward pulling force than like horizontal stiffness. In figure 17(*b*), there is an additional feature of re-entrance associated with the critical stiffness–temperature curve as the temperature is increased at fixed stiffness strength: for fixed stiffness strengths Δ_y just larger than 1 the system starts in a desorbed phase near zero temperature moving through the adsorbed phase at intermediate temperatures and then moving back to the desorbed phase at high temperatures. There is an observed maximum in the stiffness–temperature curve implying that there exists an upper bound on vertical stiffness

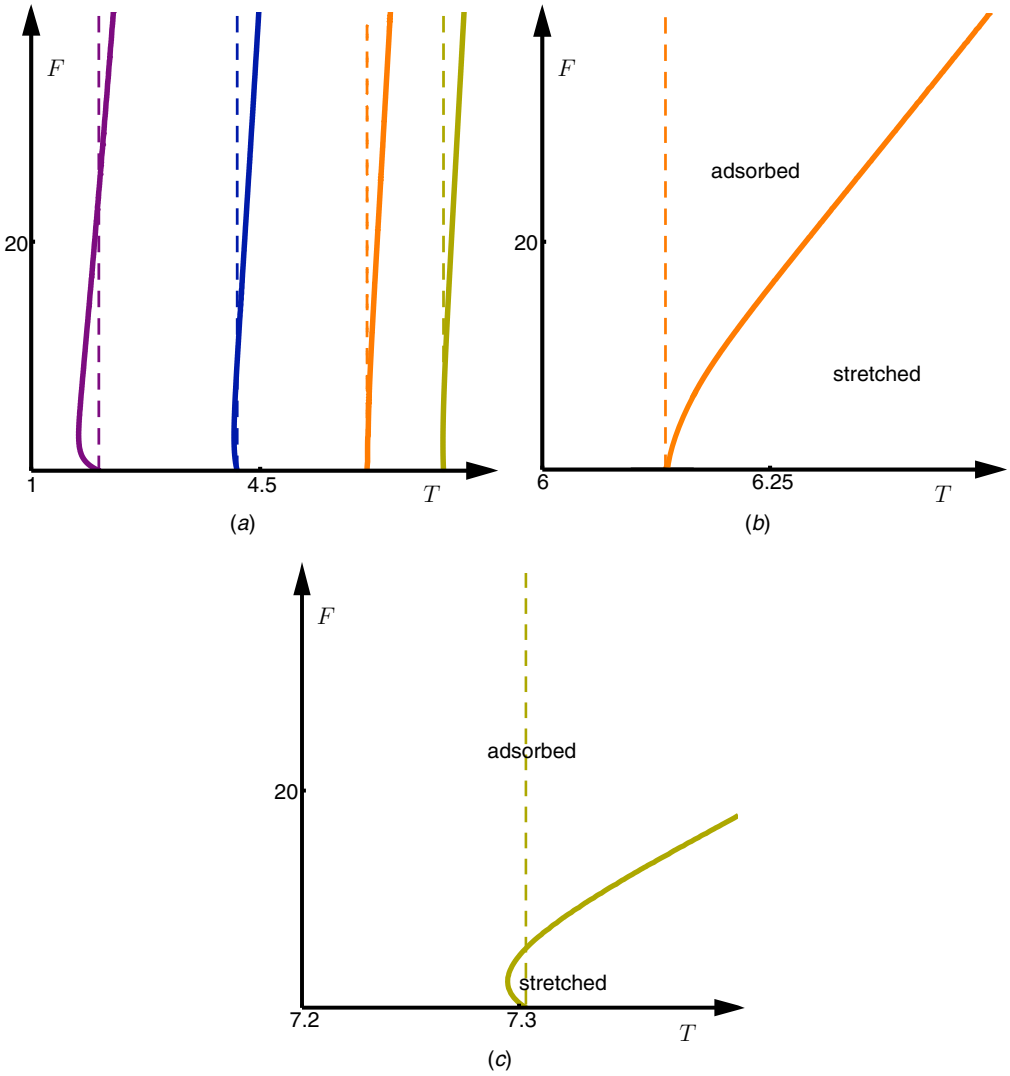

Figure 16. The general stiffness model with $r = 0$ (horizontal-only stiffness) and both horizontal and vertical pulling: The force–temperature critical curve at a fixed pulling angle $\theta = 44^\circ$ for a range of different stiffness values. (*a*) Starting from the leftmost (purple) curve, $\Delta_x = 0.2, 3, 6$ and 8. (*b*) The same plot restricted to the region $6 < T < 6.5$, showing only the critical curve with corresponding stiffness $\Delta_x = 6$. (c) Again the same plot with $7.2 < T < 7.4$, now only showing the curve with stiffness $\Delta_x = 8$. For all three figures, the corresponding dashed vertical line extends out from the zero-force critical temperature to aid visual inspection of the shape of the critical curve.

$\Delta_y{}^\star$ beyond which the system exhibits *no phase transition* on varying the temperature. Hence there is re-entrance for all fixed $1 < \Delta_y < \Delta_y{}^\star$, where vertical stiffness aids adsorption.

Specifically, in this instance when normalizing the attractive contact energy $J = 1$ we find $\Delta_y{}^\star \approx 1.0534$. Moreover, as vertical stiffness otherwise promotes desorption, a physical argument for why such re-entrance in this instance is observed would be of interest. Thus, overall, while we conclude that in the case of vertical stiffness with no pulling, the model

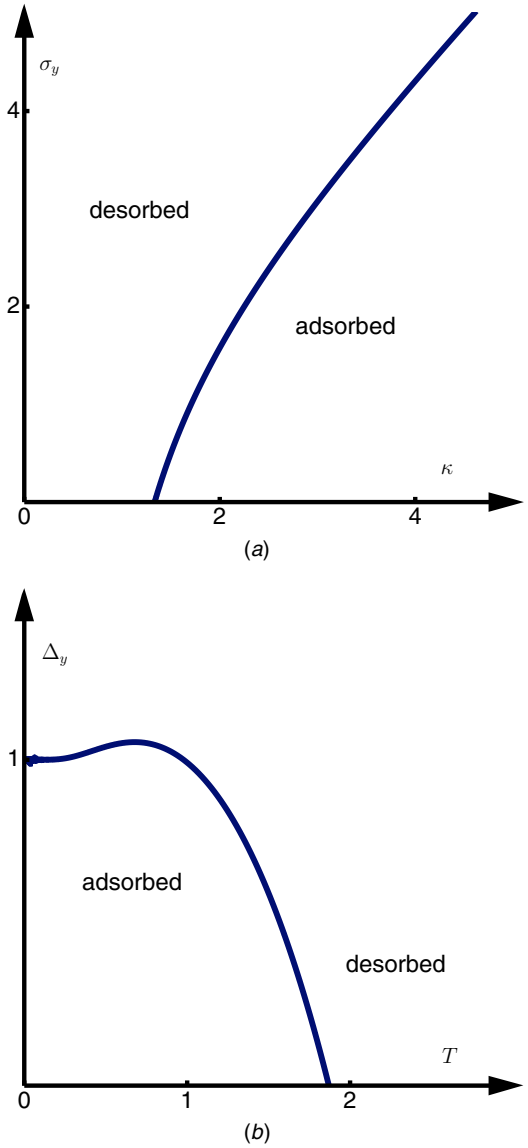

Figure 17. The general stiffness model with $r = 1$ (vertical-only stiffness) and no pulling: the system phase diagram plotted in terms of the (*a*) Boltzmann factors σ_y against κ; and in terms of (*b*) the physical variables Δ_y against T. Note the re-entrance for finite T in (*b*) for any stiffness strength Δ_y just greater than 1.

exhibits a *second order* adsorption phase transition; the physical behaviour of this model is distinct from previously studied stiffness models with stiffness ratios $r = 0$ and 0.5.

6.4.2. Vertical-only stiffness with pulling: $r = 1$, variable θ. Recall in section 5.2, that we similarly determined that the general stiffness model with pulling exhibits a *first-order* adsorption phase transition for any stiffness ratio $0 \leqslant r \leqslant 1$. Thus, we consider the physical analysis of the model, substituting $r = 1$ into (43) to describe the vertical-only stiffness critical

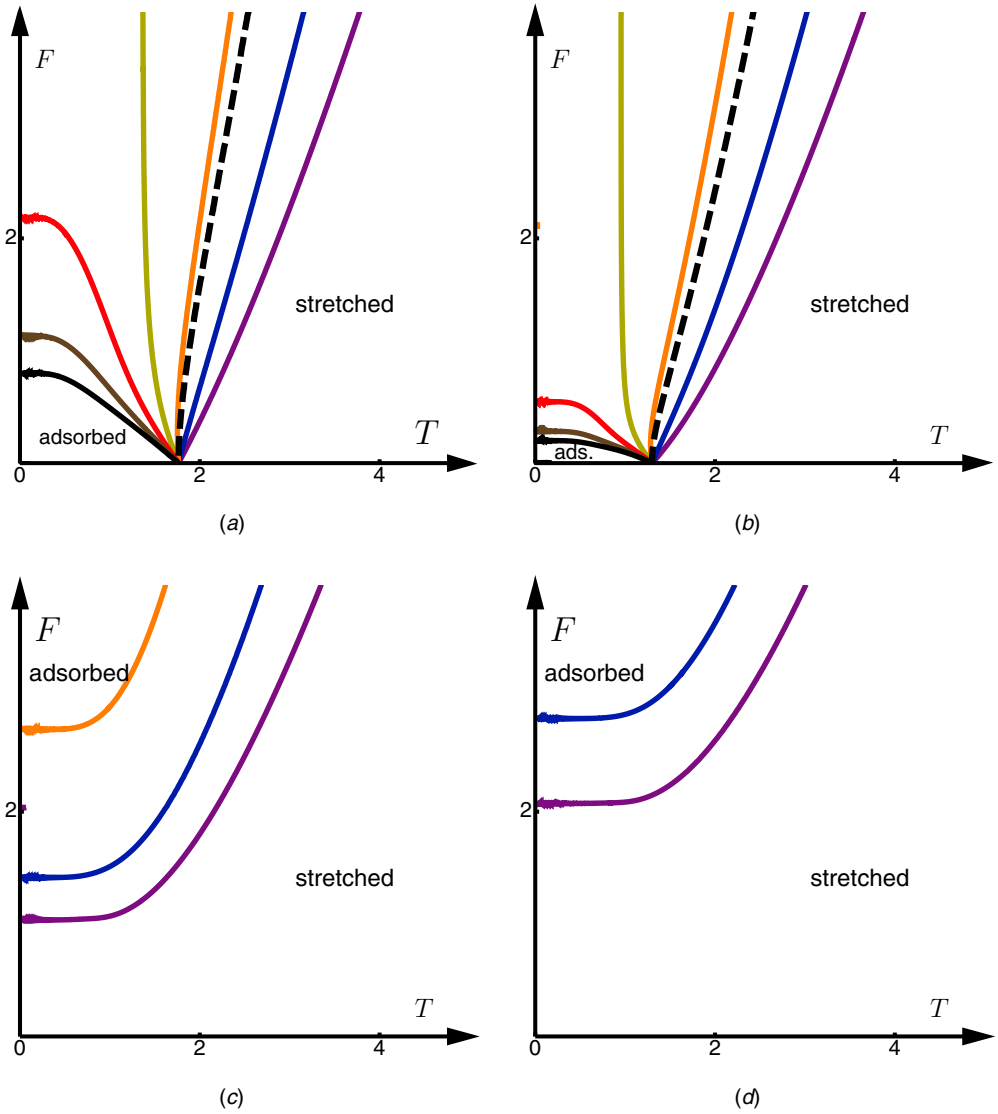

Figure 18. The general stiffness model with $r = 1$ (vertical-only stiffness) and both horizontal and vertical pulling: The temperature-force critical curve at different upward pulling angles with the stiffness attractive energy Δ_y fixed at (*a*) 0.2, (*b*) 0.8 (*c*) 2 and (*d*) 3. For each plot, starting from the right-most (purple) curve, the individual curves corresponding to an upward pulling angle of 0°, 15°, 30°, 45°, 60°, 75° and 90° away from the surface respectively. Additionally, we plot the dashed critical curve that corresponds to pulling a polymer at the separating angle (where possible).

surface for a non-zero pulling force. Here, we again plot the force–temperature critical curves in figure 18, fixing both Δ_y and θ over a range of considered values. We find the location of the zero-force critical temperatures to be: (a) $T^c_{\Delta_y=0.2} \approx 1.763\,14$ and (b) $T^c_{\Delta_y=0.8} \approx 1.299\,85$; while for cases (c) and (d) where $\Delta_y = 2$ and $\Delta_y = 3$ respectively we observe no zero-force phase transition. This reaffirms our finding in section 6.4.1, where it was indeed observed that the system exhibits no transition for $\Delta_y > \Delta_y^\star \approx 1.0534$ when normalizing the surface contact energy $-J = -1$ and ignoring pulling. Thus, we can only find the separating angle

for cases (*a*) and (*b*) where $\theta^{s}_{\Delta_y=0.2} \approx 26.6743^\circ$ and $\theta^{s}_{\Delta_y=0.8} \approx 25.9689^\circ$ respectively. By an exact argument seen for the model with no stiffness effects in section 2, we again claim that the force–temperature critical curves at corresponding pulling angles between 0° and $\theta^{s}_{\Delta_y}$ describe the force required to definitely induce adsorption. Thus, we observe that an increase in vertical stiffness *decreases* the range of pulling angles that are guaranteed to shift the system from a desorbed to adsorbed phase given enough pulling force. Moreover, we similarly find that pulling a polymer between the angles of $\theta^{s}_{\Delta_y}$ up to 45° can induce either adsorption or desorption. However, for $\Delta > \Delta_y{}^\star$, we no longer observe a zero-force critical temperature nor separating angle, with the system lying in a desorbed phase for all $T > 0$, $F = 0$. In this instance, we require a pulling angle below 45° where the horizontal force pulling component is greater than its vertical counterpart in order to observe a critical point as is seen in figures 18(*c*) and (*d*). Specifically, when $\Delta > \Delta_y{}^\star$, *any* pulling angle below 45° will be capable of inducing adsorption given a large enough pulling force.

Note, that we have only thus-far considered the two instances where $\Delta_y < 1$ and $\Delta_y > \Delta_y{}^\star$. However, it was found in section 6.4.1 that the zero-force phase diagram with respect to Δ_y and T exhibits re-entrance, resulting in the existence of a lower and upper critical temperature $T^{c,l}_{\Delta_y}$ and $T^{c,u}_{\Delta_y}$ respectively for fixed Δ_y in the range $1 < \Delta_y < \Delta_y{}^\star$ when $J = 1$. In the temperature range $T^{c,l}_{\Delta_y} < T < T^{c,u}_{\Delta_y}$ the system is in the adsorbed phase. Thus, we consider Δ_y lying in this region $1 < \Delta_y < \Delta_y{}^\star$ and plot in figures 19(*a*) and (*c*) the force–temperature critical curves with fixed $\Delta_y = 1.025$ for a number of fixed pulling angles ranging from (*a*) $\theta \geqslant 45^\circ$ and (c) $0 \leqslant \theta < 45^\circ$ respectively. Here, for the case of no pulling force, the system lies in a *desorbed* phase for temperatures lying in either $0 < T < T^{c,l}_{\Delta_y=1.0125} \approx 0.404\,074$ or $T > T^{c,u}_{\Delta_y=1.0125} \approx 0.900\,947$; while the polymer remains adsorbed for $T^{c,l}_{\Delta_y=1.0125} < T < T^{c,u}_{\Delta_y=1.0125}$. With that in mind, we can begin to interpret the behaviour of the critical curves in figure 19(*a*) where $\theta \geqslant 45^\circ$. In this instance, we find that pulling a polymer at such an angle can *only* induce desorption, with critical curves wedged between the lower and upper zero-force critical temperatures and that exhibit a local maximal critical point. Such behaviour is additionally observed in figure 19(*b*), where we increase vertical stiffness $\Delta_y = 1.04$ (with the angle remaining greater than or equal to 45°); and in general we find such behaviour is consistent for all $1 < \Delta_y < \Delta_y{}^\star$. Moreover, expectantly, we find that as $\Delta_y \to \Delta_y{}^\star$, such curves exhibit a smaller maximal critical point, as a lower predominantly vertical pulling force is required to aid vertical stiffness in inducing desorption.

Considering next the case where $1 < \Delta_y < \Delta_y{}^\star$ for pulling angles ranging between $0^\circ \leqslant \theta < 45^\circ$, we find in figure 19(*b*) where $\Delta_y = 1.025$, that such critical curves are no longer continuous. Now, while it is clear that at some pulling angles we are able to both induce adsorption and desorption for low and high pulling forces respectively, the discontinuity of the critical curves, along with the existence of two zero-force critical temperatures makes the interpretation of the lower $\theta^{s,l}_{\Delta_y}$ and upper $\theta^{s,u}_{\Delta_y}$ separating angles less straightforward relative to when $\Delta_y < 1$. Nonetheless, recalling that the corresponding critical curve at the separating angle exhibits a purely vertical slope at the zero-force critical temperature, we find that pulling a polymer at an angle $\theta < \theta^{s,l}_{\Delta_y}$ and $\theta < \theta^{s,u}_{\Delta_y}$ yields critical curves that lie immediately to the left and right of the lower and upper zero-force critical temperature respectively. Thus, around a neighbourhood centred at $T^{c,l}_{\Delta_y}\big(T^{c,u}_{\Delta_y}\big)$, such curves can *only* induce adsorption for $\theta < \theta^{s,l}_{\Delta_y}\big(\theta < \theta^{s,u}_{\Delta_y}\big)$. Moreover, beginning from $\Delta_y = 1$, where $\theta^{s,l}_{\Delta_y=1} = 0^\circ$ and $\theta^{s,u}_{\Delta_y=1} \approx 21.88^\circ$, we find that as the vertical stiffness approaches $\Delta_y{}^\star$, the lower and upper separating angles increase and decrease respectively, converging to a common angle $\theta^{s}_{\Delta_y=\Delta_y{}^\star} \approx 14.4645^\circ$. Thus, as we increase vertical stiffness, the region between the lower and upper separating angle

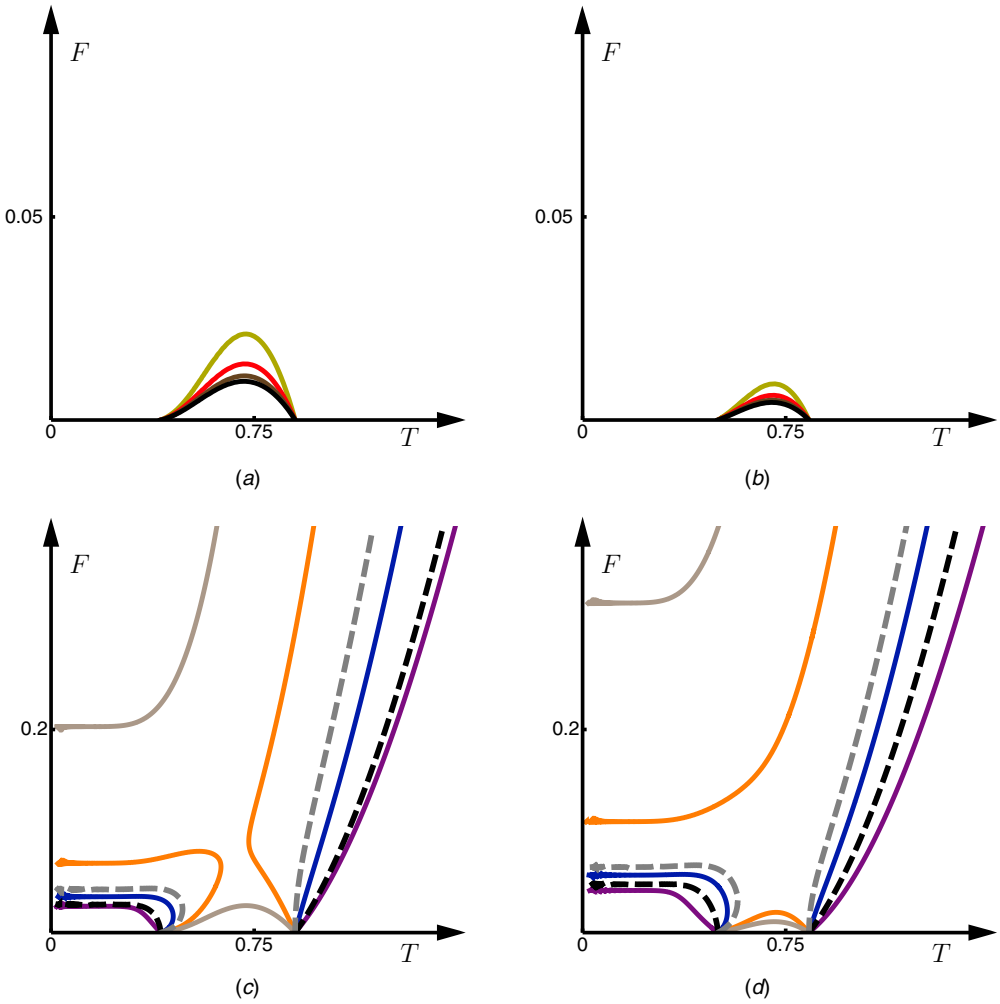

Figure 19. The general stiffness model with $r = 1$ (vertical-only stiffness) and both horizontal and vertical pulling: The temperature-force critical curve at different upward pulling angles with the stiffness attractive energy Δ_y fixed at (*a*), (*c*) 1.025 and (*b*), (*d*) 1.04. For both (*a*) and (*b*) we plot critical curves at pulling angles $\theta \geqslant 45^\circ$. In particular, starting from the top-most (yellow) curve and moving downwards we have corresponding pulling angles of 45°, 60°, 75° and 90° away from the surface respectively. Similarly, (*c*) and (*d*) plots critical curves at pulling angles $45^\circ < \theta \leqslant 90^\circ$, where starting from the bottom-left-most (purple) curve and moving upwards we have corresponding pulling angles of 0°, 15°, 20°, 30° and 40° respectively. Additionally, for (*c*) and (*d*) we include dashed critical curves for that correspond to pulling a polymer at the lower (black) and upper (grey) separating angles.

diminishes, and so a wider range of angles can induce *both* adsorption and desorption. In fact, as the maximal upper separating angle occurs when $\theta^{s,u}_{\Delta_y=1} \approx 21.88^\circ$, it is clear that pulling angles between $\theta^{s,u}_{\Delta_y=1} \approx 21.88^\circ \leqslant \theta < 45^\circ$ will *always* induce either adsorption or desorption for $1 < \Delta_y < \Delta_y{}^\star$. However, an increasing vertical stiffness also decreases the region between the upper and lower zero-force critical temperatures, similarly converging to a common point $T^c_{\Delta_y=\Delta_y{}^\star} \approx 0.671\,554$, beyond which there is no temperature region for which the system lies in a zero-force adsorbed phase. Finally, figure 19(*c*) highlights that we can classify these

critical curves as exhibiting one of two different discontinuous characteristics, as seen when comparing figure 19(*c*) with figure 19(*d*) for $\theta = 30^\circ$. Specifically, it is only in the latter case that we observe a local maximal critical point, along with an increasing component beginning at zero-temperature. Moreover, irrespective of the discontinuous behaviour, we always observe a zero-temperature critical point $F^c_{T=0}(\theta)$. Specifically, at zero temperature, we ignore entropic effects, and thus within the system we only observe rigid polymer conformations that solely comprise of a rod-like adsorbed (horizontal) and stretched (vertical) components respectively. Thus, in this instance, the free energy Ψ for a polymer with L total and n horizontal steps is given by

$$\Psi = -nJ - nF\cos\theta - (L-n)F\sin\theta - (L-n)\Delta_y. \tag{65}$$

Setting, $\partial\Psi/\partial n = 0$ and solving for F, we find the zero-temperature critical force explicitly to be

$$F^c_{T=0}(\theta) = \frac{\Delta_y - 1}{\cos(\theta) - \sin(\theta)}, \tag{66}$$

where we recall that we normalized the surface contact energy $J = 1$. From (66), it is thus clear that for $\Delta_y < 1$, $F^c_{T=0} > 0$ for pulling angles between $45^\circ < \theta < 90^\circ$; while for $\Delta_y > 1$, $F^c_{T=0}$ is positive when $0^\circ < \theta < 45^\circ$, which is consistent with our observations in figures 18 and 19. Beyond the zero-temperature critical force, we additionally find that as $\Delta_y \to \Delta_y^\star$, these critical curves begin to transition from the first to second type of discontinuity as seen in figure 19(*b*). In particular, an increase in vertical stiffness from $\Delta_y = 1.025$ to $\Delta_y = 1.04$ results in a shift in the behaviour of the curve with corresponding pulling angle $\theta = 30^\circ$. Now, while in general finding the precise location for when these curves transition is intractable, we have the necessary condition that $\theta > \theta^{s,u}_{\Delta_y}$—that is, that we require pulling at such an angle to be capable of inducing either adsorption or desorption for $1 < \Delta_y < \Delta_y^\star$ around *both* zero-force critical temperatures. Thus as the lower and upper separating angles converge to $\theta^s_{\Delta_y=\Delta_y^\star} \approx 14.4645^\circ$, such a condition implies that we will *never* observe critical curves with a local maximum for pulling angles ranging between $0^\circ \leqslant \theta \leqslant 14.4645^\circ$. Again, we should recall that for $\Delta_y > \Delta_y^\star$, pulling a polymer can only induce adsorption (for $\theta < 45^\circ$), reverting back to *continuous* critical curves as seen in figures 18(*c*) and (*d*).

6.5. General stiffness ratio: $0 \leqslant r \leqslant 1$

Having considered the horizontal-only ($r = 0$), equal ($r = 0.5$) and vertical-only ($r = 1$) stiffness models, we are now in a more convenient position to describe the physical behaviour of the general stiffness model for any stiffness ratio $0 \leqslant r \leqslant 1$ both without and with pulling.

6.5.1. General stiffness ratio with no pulling: $0 \leqslant r \leqslant 1$, $F = 0$. We begin by plotting the phase diagram in figure 20 both in terms of Boltzmann factors and physical variables, observing the effect that the stiffness ratio has on the critical curve. In particular, in figure 20(*a*), we find that all curves intersect at a common critical point when $\sigma = 1$ and thus $\kappa_{a=s} = 1 + 1/\sqrt{2}$. Let the critical temperature for $\Delta = 0$ be denoted $T_0^c = J/\log(\kappa_{a=s})$. Here, if $\sigma = 1$, stiffness effects are ignored and thus the critical point is independent of the stiffness ratio. Interestingly, in figure 20(*b*), showing the phase diagram with respect to temperature T and the potential stiffness energy Δ, we note that *only* critical curves with a corresponding stiffness ratio $r > 0.5$ exhibit a *zero-temperature* critical point. Specifically, again by a zero-temperature argument, we ignore entropic effects, so that the free energy Ψ for a polymer consisting of L total and n horizontal steps is

$$\Psi = -nJ - n(1-r)\Delta - (L-n)r\Delta. \tag{67}$$

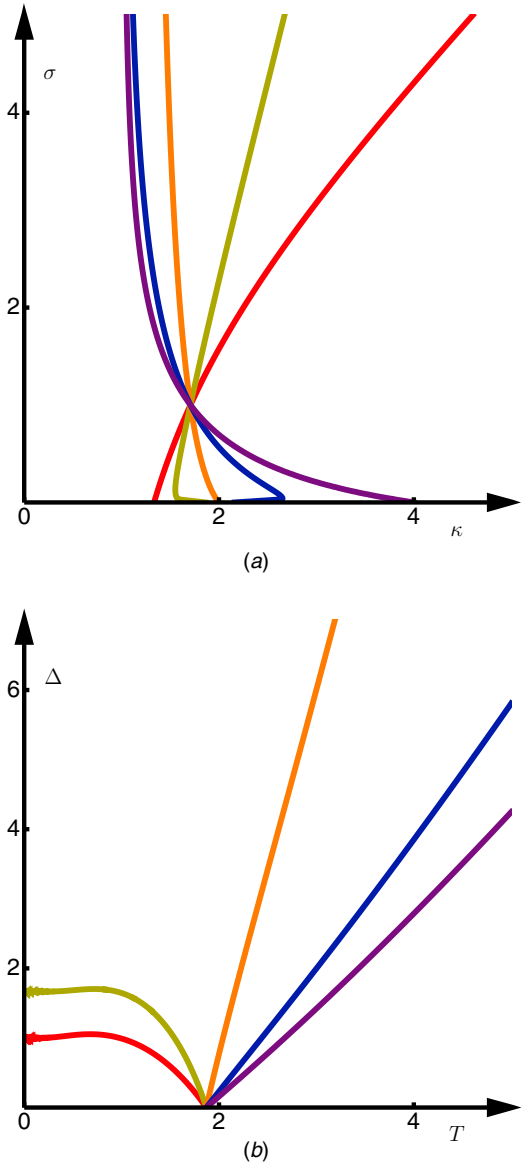

Figure 20. The general stiffness model with no pulling: the phase diagram plotted in terms of (*a*) the Boltzmann factors κ against σ for stiffness ratios, starting with the top left-most (purple) curve, of $r = 0, 0.2, 0.5, 0.8$ and 1; and in terms of (*b*) the physical variables T (temperature) against Δ (stiffness energy), again with stiffness ratios, starting right-most, of $r = 0, 0.2, 0.5, 0.8$ and 1. The system is in the desorbed phase for sufficiently high temperatures.

Now, setting $\partial\Psi/\partial n = 0$ and solving for Δ, we find the zero-temperature critical stiffness to be

$$\Delta^c_{T=0}(r) = \frac{1}{2r-1}. \tag{68}$$

Moreover, this result, in combination with the observation that the critical curve for the case of equal horizontal and vertical stiffness ($r = 0.5$) is positively-sloping for all Δ, allows

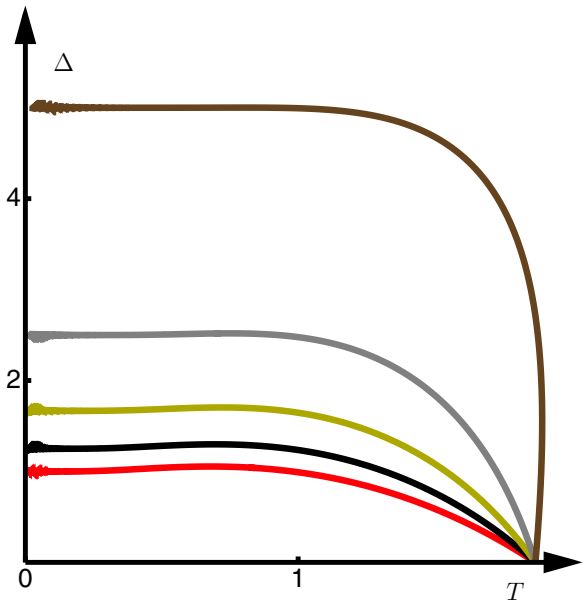

Figure 21. The general stiffness model with no pulling: the phase diagram in terms of T (temperature) against Δ (stiffness energy), for corresponding stiffness ratios, starting left top-most (brown curve) and moving downwards, of $r = 0.6, 0.7, 0.8, 0.9$ and 1. The system is in the desorbed phase for sufficiently high temperatures.

us to claim that we can *never* observe a critical temperature that is constant as a function of Δ for any $0 \leqslant r \leqslant 1$. Instead, we either have an increasing critical temperature ($0 \leqslant r \leqslant 0.5$) as Δ is increased or a critical curve that curls back to the axis, exhibiting a zero-temperature critical point ($0.5 < r \leqslant 1$). We note that there is a set of values of r just greater than $1/2$ such that at fixed temperatures just larger than T_0^c the system moves as the stiffness strength is increased from the desorbed phase at low stiffness strengths through adsorbed phase at intermediate stiffness strengths back to the desorbed phase for large stiffness strengths: see the curve associated with $r = 0.6$ in figure 21.

In figure 20(*b*) we observe that the critical curves for which $r > 0.5$ also exhibit re-entrance for fixed Δ as temperature is varied and there exist a local maximal value $\Delta_r^\star > \Delta_{T=0}^c$ beyond which there is no zero-force phase transition. Indeed, in figure 21 we plot a greater number of critical curves with stiffness ratio $r > 0.5$ to showcase such behaviour. Here, considering both the location of the stiffness upper-bound $\Delta_r^\star$ as well as the *difference* between this bound and the critical zero-temperature stiffness $\delta\Delta_r^\star \equiv \Delta_r^\star - \Delta_{T=0}^c$ we find that: $\Delta_{r=0.6}^\star, \delta\Delta^\star \approx 5.0015, 0.0015$; $\Delta_{r=0.7}^\star, \delta\Delta^\star \approx 2.5185, 0.0185$; $\Delta_{r=0.8}^\star, \delta\Delta^\star \approx 1.7037, 0.0370$; $\Delta_{r=0.9}^\star, \delta\Delta^\star \approx 1.2984, 0.0484$; and of course, the vertical-only stiffness case $\Delta_{r=1}^\star, \delta\Delta^\star \approx 1.0543, 0.0543$. Thus, while an increase in $r > 0.5$, decreases $\Delta_r^\star$, the difference between this upper-bound and the critical zero-temperature stiffness grows larger. So as we approach the vertical-only stiffness model, there exists a *greater* range of stiffness values between $\Delta_{T=0}^c(r)$ and $\Delta_r^\star$ that can shift the system from a desorbed to adsorbed phase for low, increasing temperature.

Let us now consider how changing r changes the critical temperature $T_{\Delta,r}^c$ at fixed Δ. In figure 22, we plot $T_{\Delta,r}^c$ against $0 \leqslant r \leqslant 1$ for fixed stiffness $\Delta = 0.2, 1, 2$ and 3. We see that

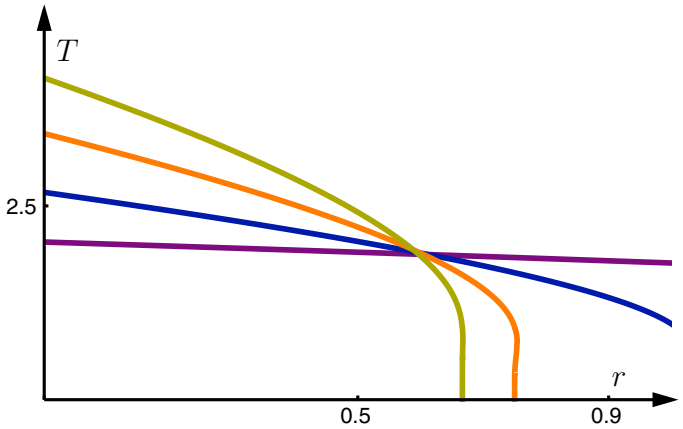

Figure 22. The general stiffness model with both horizontal and vertical pulling. The zero-force critical temperature against stiffness ratio $0 \leqslant r \leqslant 1$ for a number of fixed stiffness values. Starting from the bottom, left-most (purple) curve and moving upwards, we have curves with corresponding stiffness $\Delta = 0.2, 1, 2$ and 3 respectively.

an increase in the stiffness ratio results in a lower critical temperature, as we move towards the vertical-only stiffness model. Additionally, recall from section 6.5.1, that we asserted that all critical force–temperature curves with a corresponding stiffness ratio $0.5 < r \leqslant 1$ exhibit a critical zero-temperature point $\Delta^c_{T=0}(r)$ as well as re-entrant behaviour, giving rise to a maximal critical point $\Delta^\star_r$. Now, we can alternatively consider both the zero-temperature $r^c_{T=0}(\Delta)$ and maximal critical point $r^\star_\Delta$ as functions of r. With that in mind, for the cases where we fix $\Delta = 2$ and 3 in figure 22, we do indeed observe re-entrance, specifically finding that: $r^c_{T=0}(\Delta = 2), r^\star_{\Delta=2} \approx 0.75, 0.7537$ and $r^c_{T=0}(\Delta = 3), r^\star_{\Delta=3} \approx 0.6670, 0.6673$. Thus, as we increase Δ, a lower ratio of vertical relative to horizontal stiffness is required to ensure that we observe a zero-force critical point. Moreover, increasing stiffness further diminishes the *range* of stiffness ratios from $r^c_{T=0}(\Delta)$ to $r^\star_\Delta$ for which the system exhibits a lower $T^{c,l}_{\Delta,r}$ and upper $T^{c,u}_{\Delta,r}$ zero-force critical temperature. Again, as per the vertical-only stiffness model, both $T^{c,l}_{\Delta,r}$ and $T^{c,u}_{\Delta,r}$ converge at the maximal ratio $r^\star_\Delta$, where for the particular case of $\Delta = 2$ and 3 we have $T^c_{\Delta=2,r^\star} \approx 0.714\,137$ and $T^c_{\Delta=3,r^\star} \approx 0.728\,611$ respectively.

Considering vertical cuts of our plot corresponding to a fixed stiffness ratio, we find that an increase in Δ results in an increasing and subsequently decreasing critical temperature for low and high r respectively. Note, that while figure 22 suggests a common intersecting critical point at $r \approx 0.6$ for all chosen stiffness values, we have already established in section 6.5.1 that there exists no stiffness ratio that would yield a stationary $T^c_{\Delta,r}$ as we alter stiffness. As argued above, to reconcile these two observations there must exist a range of ratios for which the critical temperature is *not* a *strictly* increasing or decreasing function of Δ. In fact, we find that between approximately $0.5 < r < 0.621\,32$, the corresponding stiffness–temperature phase diagram is increasing and subsequently decreasing for low and high stiffness respectively.

6.5.2. General stiffness ratio with pulling: $0 \leqslant r \leqslant 1$, *variable pulling angle,* θ. With the inclusion of pulling, we are now particularly interested in the effect on the separating angle $\theta^s_{\Delta,r}$ as we alter r. We plot in figure 23, $\theta^s_{\Delta,r}$ against the stiffness ratio for fixed stiffness $\Delta = 0.2, 1, 2, 3$ and 15. Recall, that for the horizontal-only ($r = 0$) and equal-stiffness ($r = 0.5$) cases we observed an increasing and subsequently decreasing separating angle for

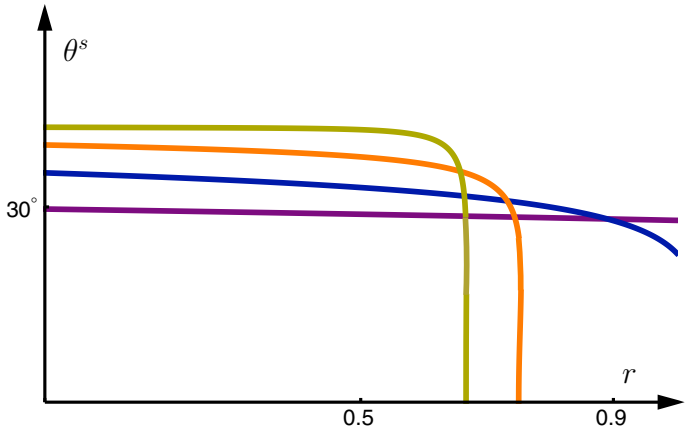

Figure 23. The general stiffness model with both horizontal and vertical pulling. The separating angle against stiffness ratio $0 \leqslant r \leqslant 1$ for a number of fixed stiffness values. Starting from the bottom, left-most (purple) curve and moving upward, we have curves with corresponding stiffness $\Delta = 0.2$, 1, 2 and 3 respectively.

low and high stiffness respectively. By considering vertical cuts in figure 23, we find that we indeed observe such behaviour for general fixed $0 \leqslant r \leqslant 0.5$, with $\theta^s_{\Delta,r} \to 0^\circ$ as $\Delta \to \infty$. Thus, for large enough stiffness, pulling a polymer at angles ranging from $0^\circ < \theta < 45^\circ$ can induce both adsorption and desorption. This implies that overall, both the horizontal and equal stiffness models are good representations of the general stiffness model where $0 \leqslant r \leqslant 0.5$. Now, for the other extreme case of vertical-only stiffness ($r = 1$), recall that increasing stiffness $\Delta_y < \Delta_y{}^\star$ *always* results in a decreasing separating angle $\theta^s_{\Delta,r=1}$. However, we clearly observe in figure 23 that for fixed $0.5 \leqslant r \leqslant 1$, our class of models instead behave like the horizontal-only and equal stiffness cases, similarly exhibiting a increasing and decreasing separating angle for low and high stiffness respectively. Thus, we have already highlighted one feature of the general stiffness model $0.5 \leqslant r \leqslant 1$ which is absent from the vertical-only stiffness case. Note, however, that as $r \to 1$ we do observe a diminishing stiffness range for which $\theta^s_{\Delta,r}$ is increasing. For instance, we find that $\theta^s_{\Delta,r}$ is increasing when $\Delta \leqslant 4.395$, 2.015 and 0.655 for stiffness ratios $r = 0.6$, 0.7 and 0.9 respectively. Thus, as $r \to 1$, the stiffness interval for which the separating angle is increasing becomes narrower, with the model approaching the behaviour of the vertical-only stiffness case. Additionally, the general stiffness model for all $0.5 < r < 1$ does share characteristics with the upper-bound $r = 1$ model. Specifically, we have already established that such models exhibit a zero-temperature critical stiffness $\Delta^c_r \equiv \Delta^c_{T=0}(r)$ as well as re-entrant behaviour with a maximal critical point $\Delta^\star_r$. With respect to the separating angle, these two characteristics give rise to a lower $\theta^{s,l}_{\Delta,r}$ and upper $\theta^{s,u}_{\Delta,r}$ separating angle for $\Delta^c_{T=0}(r) < \Delta < \Delta^\star_r$. As per the vertical-only stiffness case, $\theta^{s,l}_{\Delta=\Delta^c_r,r} = 0^\circ$ for any $0.5 < r \leqslant 1$, while we find that $\theta^{s,u}_{\Delta=\Delta^c_r,r} \approx 26.4711^\circ, 25.2365^\circ$ and 22.6343 for $r = 0.6$, 0.7 and 0.9 respectively, with the lower and upper separating angle converging to $\theta^s_{\Delta=\Delta^\star_r}$. Moreover, we similarly find that for $\Delta > \Delta^\star_r$, pulling a polymer can only induce adsorption (for $\theta < 45^\circ$). Thus, loosely speaking, for $0.5 < r < 1$, we find that $\theta^s_{\Delta,r}$ for the general stiffness model behaves more like its horizontal-only and equal-stiffness counterpart at low stiffness ($\Delta < \Delta^c_r$), while for $\Delta^c_r \leqslant \Delta < \Delta^\star_r$, we observe converging lower and upper separating angles as per the vertical-only stiffness case.

7. Conclusion

We have solved exactly by means of the kernel method a generalized partially directed walk model of a stretched semi-flexible polymer near a sticky wall in two dimensions, incorporating both horizontal and vertical stiffness effects.

We revisited previously studied model sub-cases, highlighting their key findings with respect to the model's physical variables: T temperature, F pulling force and θ the upward pulling angle away from the surface.

With our solution to the general model at hand, we identified the adsorbed, desorbed and stretched dominant singularities of the generating function. To discuss the behaviour of general model in more detail we introduced a stiffness parameter r that scaled the potential energy attributed to a vertical stiffness site as $r\Delta$ and to a horizontal stiffness site as $(1-r)\Delta$. When excluding or including pulling, we found that for all $0 \leqslant r \leqslant 1$, the general stiffness model exhibits a second or first-order adsorption phase transition respectively, allowing us to conclude that anisotropic stiffness effects do not alter the order of the adsorption phase transition.

Turning to the shape of the critical curve for the equal horizontal and vertical stiffness ($r = 0.5$) model, we found that at low stiffness, an increase in Δ increased the separating angle θ^s_Δ (the largest angle for which stretching a polymer induces only adsorption). However, when normalizing the potential energy attributed to a surface contact $-J = -1$, we found a maximal separating angle of 45° when the stiffness energy $\Delta \approx 2.239\,44$, highlighting that a pulling force with a larger vertical relative to horizontal component can never induce adsorption. Additionally, we found that as $\Delta \to \infty, \theta^s_\Delta \to 0^\circ$, implying that (eventually) an increase in stiffness, increases the range of pulling angles that can induce both desorption and adsorption.

For horizontal-only ($r = 0$) stiffness and variable pulling the system was shown to exhibit similar behaviour to that of the equal stiffness model, with a maximal separating angle $\theta^s_{\Delta_x}$ again occurring at 45°, while we observe that an increase in horizontal stiffness also *decreases* the separating angle. However, this rate of decrease is dampened relative to the equal stiffness case, showing that an increase in horizontal stiffness produces a smaller change in the range of pulling angles that can additionally induce desorption.

We have carefully analyzed the, previously unconsidered, model that incorporates vertical-only ($r = 1$) stiffness both with and without pulling. Without pulling, we found a stiffness–temperature phase diagram that is in contrast to the horizontal stiffness case, exhibiting behaviour that is much more closely related to an upward vertical pulling force acting on the free-end of a polymer. Additionally, we found that while, generally, an increase in vertical stiffness *decreases* the critical temperature, the stiffness–temperature critical curve exhibited re-entrance at low temperatures—a feature which had only previously been observed in co-polymer or three-dimensional models. Moreover, as the critical temperature does not forever decrease, we also found an upper bound stiffness $\Delta_y^\star \approx 1.0534$ beyond which the model exhibits no phase transition, further highlighting the distinctiveness of the vertical-only stiffness case. With the addition of pulling, we again found physical characteristics that differed from the horizontal and equal stiffness cases. In particular, the separating angle does not increase over any range of Δ_y, but rather an increase in vertical stiffness *always* increases the range of pulling angles from $\theta^s_{\Delta_y}$ up to 45° that can induce both adsorption and desorption (for $\Delta_y < \Delta_y^\star$).

Finally, the understanding of the three sub-cases ($r = 0$, 0.5, and 1) of our general stiffness model allowed us to frame a discussion of the general stiffness ratios $0 \leqslant r \leqslant 1$. We found that both the horizontal and equal stiffness models were good representatives for the behaviour of

the general model for any fixed ratio $0 \leqslant r \leqslant 0.5$. Specifically, in this instance, an increase in Δ always results in an increasing zero-force critical temperature, while the separating angle $\theta^s_{\Delta,r}$ similarly is increasing and subsequently decreasing for low and high stiffness respectively. Additionally, we again observed that as $\Delta \to \infty$, $\theta^s_{\Delta,r} \to 0^\circ$. Thus, in general, any model with greater horizontal relative to vertical stiffness exhibits consistent physical characteristics. Naively, one might then assume that the model's behaviour when we have a greater *vertical* relative to horizontal stiffness $0.5 < r \leqslant 1$, is captured by the vertical-only stiffness case. Indeed, we found that for all fixed $0.5 < r < 1$, the general model ignoring pulling always exhibits a re-entrant stiffness–temperature critical curve, with both a zero-temperature critical point along with a maximal critical stiffness beyond which the system exhibits no zero-force phase transition. However, the inclusion of pulling into our general model revealed behaviour that was instead more closely related to the horizontal-only case. In particular, we found that there exists a range of stiffness values for which the separating angle is *increasing*, with such a stiffness range diminishing as $r \to 1$. Thus overall, for $0.5 < r \leqslant 1$, we no longer observe consistent physical characteristics amongst all models, but rather we conclude that the behaviour of the general model approaches that of the vertical-only stiffness case as the stiffness ratio is increased towards 1.

Acknowledgments

Financial support from the Australian Research Council via its support for the Centre of Excellence for Mathematics and Statistics of Complex Systems is gratefully acknowledged by the authors. One of the authors, RT, acknowledges financial support from the University of Melbourne via its Melbourne Research Scholarships scheme.

References

[1] Ashkin A 1997 Optical trapping and manipulation of neutral particles using lasers *Proc. Natl Acad. Sci.* **94** 4853–60
[2] Banderier C and Flajolet P 2002 Basic analytic combinatorics of directed lattice paths *Theor. Comput. Sci.* **281** 37–80
[3] Bouchaud E and Vannimenus J 1989 Polymer adsorption: bounds on the cross-over exponent and exact results for simple models *J. Phys.* **50** 2931–49
[4] Bousquet-Mélou M 2002 Four classes of pattern-avoiding permutations under one roof: generating trees with two labels *Electron. J. Comb.* **9** 19
[5] Brak R, Owczarek A L, Rechnitzer A and Whittington S G 2005 A directed walk model of a long chain polymer in a slit with attractive walls *J. Phys. A: Math. Gen.* **38** 4309–25
[6] Carvalho M and Privman V 1988 Directed walk models of polymers at interfaces *J. Phys. A: Math. Gen.* **21** L1033–7
[7] Essevaz-Roulet B, Bockelmann U and Heslot F 1997 Mechanical separation of the complementary strands of DNA *Proc. Natl Acad. Sci.* **94** 11935–40
[8] Forgacs G 1991 Unbinding of semiflexible directed polymers in 1+1 dimensions *J. Phys. A: Math. Gen.* **24** L1099–103
[9] Grassberger P and Hegger R 1995 Simulations of three-dimensional θ polymers *J. Chem. Phys.* **102** 6881
[10] Iliev G K, Orlandini E and Whittington S G 2010 Directed walk models of adsorbing semi-flexible polymers subject to an elongational force *J. Phys. A: Math. Theor.* **43** 315202
[11] Janse van Rensburg E J, Orlandini E, Owczarek A L, Rechnitzer A and Whittington S G 2005 Self-avoiding walks in a slab with attractive walls *J. Phys. A: Math. Gen.* **38** L823–8
[12] Krawczyk J, Owczarek A L and Prellberg T 2009 Semi-flexible hydrogen-bonded and non-hydrogen bonded lattice polymers *Physica* A **388** 104–12
[13] Krawczyk J, Prellberg T, Owczarek A L and Rechnitzer A 2004 Stretching of a chain polymer adsorbed at a surface *J. Stat. Mech.* **2004** P10004
[14] Lubensky D K and Nelson D R 2000 Pulling pinned polymers and unzipping DNA *Phys. Rev. Lett.* **85** 1572–5

[15] Lubensky D K and Nelson D R 2002 Single molecule statistics and the polynucleotide unzipping transition *Phys. Rev.* E **65** 031917
[16] Marenduzzo D, Bhattacharjee S M, Maritan A, Orlandini E and Seno F 2001 Dynamical scaling of the DNA unzipping transition *Phys. Rev. Lett.* **88** 028102
[17] Marenduzzo D, Maritan A, Rosa A and Seno F 2003 Stretching of a polymer below the θ point *Phys. Rev. Lett.* **90** 88301
[18] Marenduzzo D, Maritan A, Rosa A, Seno F and Trovato A 2009 Phase diagrams for dna denaturation under stretching forces *J. Stat. Mech.* **2009** L04001
[19] Martin R, Orlandini E, Owczarek A L, Rechnitzer A and Whittington S G 2007 Exact enumeration and monte carlo results for self-avoiding walks in a slab *J. Phys. A: Math. Theor.* **40** 7509–21
[20] Mishra P K, Kumar S and Singh Y 2003 A simple and exactly solvable model for a semiflexible polymer chain interacting with a surface *Physica* A **323** 453–65
[21] Mishra PK, Kumar S and Singh Y 2005 Force-induced desorption of a linear polymer chain adsorbed on an attractive surface *Europhys. Lett.* **69** 102–8
[22] Orlandini E, Bhattacharjee S M, Marenduzzo D, Maritan A and Seno F 2001 Mechanical denaturation of DNA: existence of a low-temperature denaturation *J. Phys. A: Math. Gen.* **34** L751–8
[23] Orlandini E and Tesi M C 2009 Modelling the adsorption of a polymer subject to an elongational force by directed walk models *J. Math. Chem.* **45** 72–94
[24] Orlandini E, Tesi M C and Whittington S G 2004 Adsorption of a directed polymer subject to an elongational force *J. Phys. A: Math. Gen.* **37** 1535–43
[25] Owczarek A L 2009 Exact solution for semi-flexible partially directed walks at an adsorbing wall *J. Stat. Mech.* **2009** P11002
[26] Owczarek A L 2010 Effect of stiffness on the pulling of an adsorbing polymer from a wall: an exact solution of a partially directed walk model *J. Phys. A: Math. Theor.* **43** 225002
[27] Owczarek A L and Prellberg T 2007 Exact solution of semi-flexible and super-flexible interacting partially directed walks *J. Stat. Mech.* **2007** P11010
[28] Osborn J and Prellberg T 2010 Forcing adsorption of a tethered polymer by pulling *J. Stat. Mech.* **2010** P09018
[29] Orlandini E and Whittington S G 2010 Adsorbing polymers subject to an elongational force: the effect of pulling direction *J. Phys. A: Math. Theor.* **43** 485005
[30] Owczarek A L and Whittington S G 2009 *Interacting Lattice Polygons (Lecture Notes in Physics* vol 775*)* (Berlin: Springer) chapter 12 pp 301–15
[31] Privman V, Forgacs G and Frisch H L 1988 New solvable model of polymer-chain adsorption at a surface *Phys. Rev.* B **37** 9897–900
[32] Rosa A, Marenduzzo D, Maritan A and Seno F 2003 Mechanical unfolding of directed polymers in a poor solvent: critical exponents *Phys. Rev.* E **67** 041802
[33] Strick T, Allemand J F, Croquette V and Bensimon D 2001 The manipulation of single biomolecules *Phys. Today* **54** 46
[34] Svoboda K and Block S M 1994 Biological applications of optical forces *Annu. Rev. Biophys. Biomol. Struct.* **23** 247–85